Islands of stability and quasi-magic numbers for super- and ultra-heavy nuclei

M. Ismail[1] A. Y. Ellithi[1] A. Adel[1,3] Hisham Anwer[1,2;1)]

[1] Physics Department, Faculty of Science, Cairo University, Egypt
[2] Physics Department, German University in Cairo, New Cairo City, Egypt
[3] Physics Department, College of Science, Majmaah University, Al-Zulfi, Kingdom of Saudi Arabia

Abstract: In the framework of Strutinsky's approach, we calculated the shell and the residual pairing correction energies for 5569 even-even nuclei in the range $72 \leqslant Z \leqslant 282$ and $96 \leqslant N \leqslant 540$. Quasi-magic numbers and deformed islands of stability that reside in a range defined by Green's formula and the two-neutrons drip line are introduced. We present 36 quasi-magic proton and 53 quasi-magic neutron magic numbers that contribute to the formation of 133 deformed islands of stability along the N-Z space. The quasi-magic proton and neutron magic numbers volatile as the mass number increases and other magic numbers take over. Consequently, the deformed islands of stability fail to exhibit a pattern along the search space covered.

Keywords: deformed nuclei, islands of stability, magic numbers

PACS: 21.10.-k, 21.60.Cs **DOI:** 10.1088/1674-1137/40/12/124102

1 Introduction

Experimental results on the structure of neutron-rich isotopes have tested the assumption that magic numbers are probable for spherical as well as deformed shapes. For systems with an unbalanced proton-to-neutron ratio, the original magic numbers may disappear while others emerge. In Ref. [1], Doornenbal et al. suggested that a large area of deformation emergences in the range $N=20-28$ shell quenching. Furthermore, it was experimentally found that heavy nuclei of the actinium series ($Z=93-103$) are well deformed [2, 3]. This fact strongly suggests that deformed configurations are as important as spherical ones for stability of the heaviest nuclei. In Ref. [4], Bohr and Mottelson also pointed out that deformation can play a major role in increasing stability in the heavy regions. Muntian, Patyk, and Sobiczewski argued that superheavy nuclei around $^{270}_{162}\mathrm{Hs}_{108}$ are deformed [5]. It turned out that extracting information on deformation is crucial for understanding the structure of superheavy nuclei, especially with the advent of new tools and techniques for experimental nuclear physics. The newly developed and the upcoming experimental facilities produce even more new isotopes. Thus, the structure of superheavy nuclei is a topic of current interest which has been intensively studied in the last few years and is worthwhile to explore using various theoretical approaches.

When nuclear deformations are taken into consideration, it results in the appearance of additional minima in the shell correction energy surfaces[6–8, 10–13, 34]. Arguably, these additional minima correspond to filling of the shells in deformed nuclei and represent quasi-magic numbers. In many cases, deformation essentially provides an additional binding which attracts the system to even stronger shell stabilization [9]. Recently, many theoretical calculations were used in an attempt to find out deformed shell closures in a wide range of the nuclear landscape.

In Refs. [14–15], Patyk et al. and Möller et al. calculated an island of deformed shell closures around Z=108, respectively. In recent experiments at GSI [16, 17] and Dubna [18, 19], this region has been accessed, where among many other isotopes the region around the expected deformed doubly magic nucleus $^{270}_{162}\mathrm{Hs}_{108}$ has been reached. Furthermore, based upon the finite-range droplet model, P. Möller and J. Nix also predicted large shell gaps in the region where Z=104, 106, 108, 110 and at N=162, 164 [15].

In the framework of relativistic Hartree-Bogoliubov theory, calculations with a finite-range pairing force of Gogny effective interaction D1 and effective interaction NLSH [20] show that $Z=114$ and $N=160$, 166, 184 exhibit stability compared to their neighbors and a doubly magic character at $Z=106$ and $N=160$ is also indicated in Ref. [20]. The Skyrme-Hartree-Fock method with ef-

Received 12 July 2016, Revised 7 September 2016

1) E-mail: hisham@sci.cu.edu.eg

fective forces SkP and SLy7 predicts nuclear magicity in the region $Z = 126$ and $N = 184$, and also shows evidence of increased stability around $N = 162$ due to the deformed shell effects [21]. Based on two-nucleon gaps calculated in the framework of non-relativistic Skyrme-Hartree-Fock calculations with SkM*, SkP, SLy6, SkI1, SkI3, SkI4 effective interactions and relativistic mean field calculation with PL-40, NLSH, NL-Z, TM1 effective interactions, K. Rutz et al. [22] predicted that $^{298}114$, $^{292}120$ and $^{310}126$ are doubly magic. Besides, their analysis showed that the resulting magic numbers are force dependent.

Many other theoretical efforts based on relativistic mean-field models [9, 25–27] yield the magic number at $Z = 120$ and $N = 172$ and 184, while the relativistic model proposed in Ref. [61] results in evidence of nuclear magicity at $Z = 114$ and 120 and $N = 172$, 184, and 258. The proton numbers $Z = 106$, 114, 120, 126, 132, and 138 and neutron numbers $N = 138$, 164, 172, 184, 198, 216, 228, 238, 252, 258, and 274 were determined as possible magic numbers based on a detailed analysis of calculations performed using the relativistic Hartree-Bogolyubov theory with allowance for a continuum [31] in which eight versions are considered in parametrizing forces. The proton magicity at $Z = 114$, 120 and 138 are spherical magic numbers, and the proton magicity at $Z = 106$, 126, 132 emerge only when the deformations are allowed.

A variety of theoretical approaches were used in studying nuclear magicity and identifying the exact location of the islands of stability along the nuclear landscape. Evidence of nucleon magicity can be inferred from the discontinuities which appear in the vicinity of the magic numbers in quantities like the separation energy, energy gap, the energies of α and β transitions, shell correction energy, pairing correction, effective pairing gap, binding energy and the excitation energies of low-lying vibrational states. Evidently, when the shell correction surfaces are plotted as function of the nucleon number, deep local minima appear in the vicinity of magic numbers [25, 31, 34, 43]. On the other hand, the residual pairing correction energy is found to have a similar characteristic to other shell correction quantities when studied as a function of the nucleon number. Where the Fermi level energy is increased, the pairing energy takes large negative values, but it approaches zero close to the shell closures [31, 32, 34]. Thus, peaks in the residual pairing correction energy surfaces or vanishing of the pairing energy can both be valuable tools in inferring nucleon magicity. The vanishing of the pairing correlations has been already considered as an evidence on nucleon magicity in many studies [31, 34, 38], and as an example, in Ref. [42], nucleon magicity was found by exploring signatures in the pairing energies of protons and neutrons evaluated within the spherical Hartree-Fock-Bogolyubov approach framework. Furthermore, in Ref. [31], the pairing energies were evaluated using the Relativistic Continuum Hartree-Bogoliubov method and showed good reliability as a deciding tool in specifying the precise location of magic numbers for protons and neutrons.

In this work, we employ the calculations of the shell correction energy and the residual pairing correction energy to study quasi-magicity and deformed islands of stability. We shall call a magic number a quasi-magic number if and only if it appears only when nuclear deformations are taken into account. We will study the region in the N-Z space with $72 \leqslant Z \leqslant 282$ and $96 \leqslant N \leqslant 540$ for nuclei that reside in a range defined by Green's formula and the two-neutron drip line. Investigations of spherical magic numbers and spherical islands of stability in this region of the nuclear landscape have already been introduced in Ref. [32]. Magic numbers that appear only when nuclear deformations are taken into account are of exceptional interest, and have been previously explored in many studies, among which are those by P. Möller et al. [15], G. Lalazissis [20], W. Zhang et al. [31] , Roger A. Rydin [53], J. H. Hamilton et al. [54], H. F. Zhang et al.[55], Yu. Oganessian [56], R. K. Gupta et al. [57], S. Liran et al. [58], D. N. Poenaru et al. [59] and Raj K. Gupta [60]. Furthermore, accessing the deformed island of stability centered around $^{270}_{162}\mathrm{Hs}_{108}$ has urged more theoretical efforts for exploring possible islands of deformed magicity along the nuclear landscape. The theoretical framework of both the shell and residual pairing correction energy is introduced in Section 2. In Section 3, we discuss in detail the obtained results and its implications. A summary and conclusion is presented in Section 4.

2 Theoretical framework

2.1 Shell correction energy methodology

In predicting the structural properties of nuclei along the nuclear landscape, strong evidence can be inferred from the shell correction energy calculations. The shell structure at the magic numbers for protons and neutrons strongly appeals with the presence of deep minima in the shell correction energy surface. Originally, the shell correction arises to compensate for the deviation from the uniform distribution of nucleons. In Strutinsky's approach, the shell correction energy is calculated as follows [6, 34]:

$$\delta E_{\rm shell} = 2\sum_{i=1}\varepsilon_i - \tilde{E}_{\rm S.P.}, \tag{1}$$

where ε_i is the single particle (S.P.) energy and $\tilde{E}_{\rm S.P.}$ is the smooth S.P. energy. $\tilde{E}_{\rm S.P.}$ is usually calculated using the Gauss-Hermite folding procedure [6, 11, 24, 34–36].

In calculating the S.P. energies, ε_i, one diagonalizes the following Hamiltonian [37]:

$$H = \hat{H} + V + V_{\rm so} + V_{\rm C} \tag{2}$$

where $\hat{H}$ is the kinetic energy operator, V is the Woods-Saxon potential, $V_{\rm so}$ is the spin-orbit potential, and $V_{\rm C}$ is the Coulomb potential[37]. The deformed Woods-Saxon potential with axial symmetry is defined with the help of the equation of nuclear surface. The nuclear surface is parameterised in terms of quadrupole (β_2), octupole (β_3), hexadecapole (β_4) and tetrahexacontapole (β_6) degrees of freedom using the relation:

$$R(\cos\theta,\hat{\beta}) = c(\hat{\beta})\ R_0\ [1+\beta_2 Y_{20}+\beta_3 Y_{30}+\beta_4 Y_{40}+\beta_6 Y_{60}] \tag{3}$$

in which $R(\theta)$ is the distance of a point on the nuclear surface from the origin of the coordinate system, $c(\hat{\beta})$ is determined from the condition that the volume, included inside the nuclear surface, is constant and independent of deformation (this volume is set equal to the volume of the corresponding spherical nucleus), $R_0 = r_0 A^{1/3}$, and $Y_{20}(\cos\theta)$, $Y_{30}(\cos\theta)$, $Y_{40}(\cos\theta)$ and $Y_{60}(\cos\theta)$ are the spherical harmonics. The deformed single-particle potential is defined by [37]:

$$V = \frac{\bar{V}}{1+\exp[{\rm dist}(\vec{r},r_0,\beta_2,\beta_3,\beta_4,\beta_6)/a]}, \tag{4}$$

where ${\rm dist}(\vec{r},r_0,\beta_2,\beta_3,\beta_4,\beta_6)$ is equal to the distance of a given point $\vec{r}$ to the nuclear surface represented by Eq. (3) and a is the diffuseness parameter. The depth of the central potential is parameterized as:

$$\bar{V} = V_0[1 \pm \kappa(N-Z)/(N+Z)] \tag{5}$$

with the plus sign for protons and the minus sign for neutrons. The values of the constants V_0 and κ as well as the radius, r_0 , and the diffuseness, a , are listed using a universal set of parameters in Table 1. The spin-orbit part of the potential is taken to be related to the central potential as follows [37]:

$$V_{\rm so} \approx \lambda \left(\frac{\hbar}{2Mc}\right)^2 \left(\vec{\nabla} V|_{r_0=(r_0)_{\rm so}}\right)\cdot\left(\vec{\sigma}\times\vec{P}\right) \tag{6}$$

where λ denotes the strength of the spin-orbit potential, M is the nucleonic mass, the vector operator $\vec{\sigma}$ composed of the Pauli matrices is connected with the nucleon spin operator $\vec{S}$ by the usual relation $\vec{S} = \frac{1}{2}\vec{\sigma}$, and $\vec{P}$ is the linear momentum operator. The depth of the central potential is parameterized as follows:

$$\bar{V} = V_0[1 \pm \kappa(N-Z)/(N+Z)] \tag{7}$$

where the plus sign for protons and the minus sign for neutrons and the values of constansts V_0 and κ are indicated in Table 1. As argued in Ref. [2], the radius parameters for the central and spin-orbit part of the potential, r_0 and $(r_0)_{\rm so}$, respectively, must be, different in general as in Table 1.

In his approach, Strutinsky introduced both the smoothed S.P. energy and the smoothed energy level $\tilde{\lambda}$ in terms of a smoothed level density $\tilde{g}(\varepsilon)$ as follows:

$$\tilde{E}_{\rm S.P.} = 2\int_{-\infty}^{\tilde{\lambda}} \varepsilon\tilde{g}(\varepsilon){\rm d}\varepsilon, \tag{8}$$

$$N(P) = 2\int_{-\infty}^{\tilde{\lambda}} \tilde{g}(\varepsilon){\rm d}\varepsilon. \tag{9}$$

Here $N(P)$ represents the neutrons (protons) number and $\tilde{g}(\varepsilon)$ takes the following form:

$$\tilde{g}(\varepsilon) = \frac{1}{\gamma\sqrt{\pi}}\sum_i \exp(-(\varepsilon-\varepsilon_i)^2/\gamma^2), \tag{10}$$

where γ is a smoothing parameter. Later, the expression of $\tilde{g}(\varepsilon)$ is proved to be γ-dependent. As a resolution to this problem, a smoothing function of the following form is introduced:

$$f(x) = \frac{1}{\sqrt{\pi}}\exp(-x^2)L_m^{1/2}(x^2), \tag{11}$$

where m is the order of the generalized Laguerre polynomial. Thus, by folding the exact S.P. level density with the smoothing function of Eq. (11) the modified $\tilde{g}(\varepsilon)$ takes the following form [6, 34]:

$$\tilde{g}(\varepsilon) = \frac{1}{\gamma}\int_{-\infty}^{\infty} {\rm d}\varepsilon' g(\varepsilon') f\left(\frac{\varepsilon-\varepsilon'}{\gamma}\right). \tag{12}$$

Arguably, it is always possible to obtain a specific range for γ and m where $\tilde{E}_{\rm S.P.}$ is independent of γ and m for different potentials [6, 7, 28, 28, 30, 34].

2.2 Residual pairing correction energy methodology

Since its first use, the concept of pairing energies proved to be fairly successful in accounting for the pairing correlations of nucleons in finite nuclei, and it was shown to be essential in the Bardeen-Cooper-Schrieffer (BCS) theory of superconductivity [40, 41]. In calculating the residual pairing correction energy, we adopted the BCS method. Let us first introduce the effective strength of the pairing interaction G, which can be defined in one of the following forms:

$$\frac{2}{G} = \sum_{\alpha=n-n_{\rm c}}^{n+n_{\rm c}} \left[(\varepsilon_\alpha-\lambda)^2+\Delta^2\right]^{-1/2}, \tag{13}$$

$$\frac{2}{G}=\int_{\tilde{\lambda}-\Omega}^{\tilde{\lambda}+\Omega}\frac{\tilde{g}(E)\mathrm{d}E}{\sqrt{(E-\tilde{\lambda})^2+\tilde{\Delta}^2}}\approx 2\tilde{g}(\tilde{\lambda})\ln\left(\frac{2\Omega}{\tilde{\Delta}}\right), \quad (14)$$

where ε_α are the microscopic Hamiltonian eigenvalues, λ is the Fermi level, Δ is the energy gap parameter, n_c accounts for the number of states involved in the interaction and $\Omega=n_\mathrm{c}/\tilde{g}(\tilde{\lambda})$ where $\tilde{g}(\tilde{\lambda})$ is the average level density at the Fermi energy. The corresponding energy gap parameter for a uniform model distribution of the single-particle states is described phenomenologically by means of the smoothed distribution gap parameter $\tilde{\Delta}$. Using $\tilde{\Delta}$ as an input parameter is found to be convenient, as the value of $\tilde{\Delta}$ does not change too much throughout the Periodic Table[34, 38]. Here we use the following form for $\tilde{\Delta}$

$$\tilde{\Delta}=\frac{12.0}{\sqrt{A}}\ \mathrm{MeV} \quad (15)$$

which is proved to give a good agreement, throughout the periodic table, between the theoretical calculations of the energy gap Δ and the corresponding experimental data [11].

The BCS equations must be solved with the constraint that the particle number, $N=2\sum_v \nu_v^2$, is conserved. Here we have:

$$\nu_v^2=\frac{1}{2}\left(1-\frac{\varepsilon_\nu-\lambda}{\sqrt{(\varepsilon_\nu-\tilde{\lambda})^2+\tilde{\Delta}^2}}\right). \quad (16)$$

Therefore, Eq. (13) and Eq. (16) are the deciding system of equations in evaluating both the Fermi level λ and the gap parameter Δ. The residual pairing correction energy can be calculated as $\delta E_\mathrm{pairing}=E_\mathrm{pair}-\tilde{E}_\mathrm{pair}$ where the energy of the pairing corrections, E_pair and the pairing correlation energy for the uniform distribution $\tilde{E}_\mathrm{pair}$ take the following forms[34, 38, 39]:

$$E_\mathrm{pair}=\sum_\nu(\varepsilon_\nu-\lambda)\mathrm{sign}[\varepsilon_\nu-\lambda_0]-\frac{(\varepsilon_\nu-\lambda)^2+\frac{1}{2}\Delta^2}{\sqrt{(\varepsilon_\nu-\lambda)^2+\Delta^2}}, \quad (17)$$

$$\tilde{E}_\mathrm{pair}=-\frac{1}{2}\tilde{g}(\tilde{\lambda})\tilde{\Delta}^2. \quad (18)$$

When varied as a function of the proton and neutron numbers the residual pairing correction energy surface show a fluctuating character, arguably involving evidence of the shell structure of protons and neutrons. The vanishing of the pairing correction energy or maxima in the residual pairing correction energy surface are strong evidence in exploring proton and neutron magic numbers along the nuclear landscape [31, 33, 34, 38, 42].

3 Results and discussion

Based on the methodology explained in the previous section, we calculated the shell and pairing correction energies for even-even nuclei with $72\leqslant Z\leqslant 282$, $96\leqslant N\leqslant 540$ and mass numbers lie between $168\leqslant A\leqslant 822$. In calculating the shell correction energy, we employ a basis formed by oscillator wave functions for the 19 shells of an axially deformed harmonic oscillator. The degree of the correcting polynomial is chosen to be six. This choice is found to be adequate in calculating shell corrections for medium mass, heavy, and superheavy nuclei [34, 43]. In Table 1, we introduce the universal Woods-Saxon parameters used in the calculations. Furthermore, the smoothing parameter γ is chosen such that $\gamma\gtrapprox\hbar\omega\approx 7-10$ MeV, and the average energy distance between neighboring major shells of a harmonic oscillator spectrum is represented by $\hbar\omega\approx 41/A^{1/3}$ [29]. The energies of single-particle levels of nucleons are calculated based on the WSBETA code [37]. We used a dynamical method to minimize the shell-plus-pairing correction energy in three dimensional deformation space namely; quadrupole β_2, octupole β_3 and hexadecapole β_4 deformations. Guided by the general trends of the ground state deformations in the databases reported by Möller et al. [44, 45], Audi et al. [46], Goriely et al. [47] and Kowal et al. [48], we let the quadrupole deformation parameter β_2 to vary in the range $\beta_2=-0.6$:0.6(0.01), the hexadecapole deformation parameter to vary in the range $\beta_4=-0.4$:0.4(0.01), and the octupole deformation parameter β_3 to vary in the range $\beta_3=0$:0.2(0.01). The shell and pairing correction energies do not feel the sign of β_3, thus we consider only positive values for the octupole deformation parameter. We restrict our study to nuclei that lie in the range between N_G-10 and two neutrons drip line, where N_G is defined by Green's formula [44, 49] as follows:

$$N_\mathrm{G}-Z=\frac{0.4A^2}{A+200}, \quad (19)$$

in which N_G is taken to be the nearest even number corresponding to a given atomic number Z. In finding out the two neutrons drip line, we calculated the two neutron separation energy S_{2n}, which is the energy required to remove two neutrons from a nucleus that is given as

$$S_{2n}=B(A,Z)-B(A-2,Z) \quad (20)$$

where $B(A,Z)$ and $B(A-2,Z)$ are the binding energies of nuclei having mass number and atomic number A, Z and $A-2$, Z, calculated using the modified Bethe-Weizsacker mass formula [50], respectively. At a fixed value of the atomic number Z, starting from large values of neutron number N, we decreased N in steps of two until S_{2n} becomes positive for the first time, a point at which the two neutron drip line nucleus is reached. Then, the Z

number is varied in steps of two resulting in the desired two neutron drip line.

The variation of the proton shell energy $\delta E^{\rm protons}_{\rm shell}$ for even-even nuclei with $72 \leqslant Z \leqslant 282$ and $96 \leqslant N \leqslant 540$ is illustrated as a function of the proton number Z for different isotopes in Fig. 1.

Table 1. Universal Woods-Saxon parameters [23].

particles	V_0/MeV	κ	r_0/fm	a/fm	λ	$(r_0)_{\rm so}$/fm	$(a)_{\rm so}$/fm
neutrons	−49.6	0.86	1.347	0.70	36.0	1.310	0.70
protons	−49.6	0.86	1.275	0.70	36.0	1.320	0.70

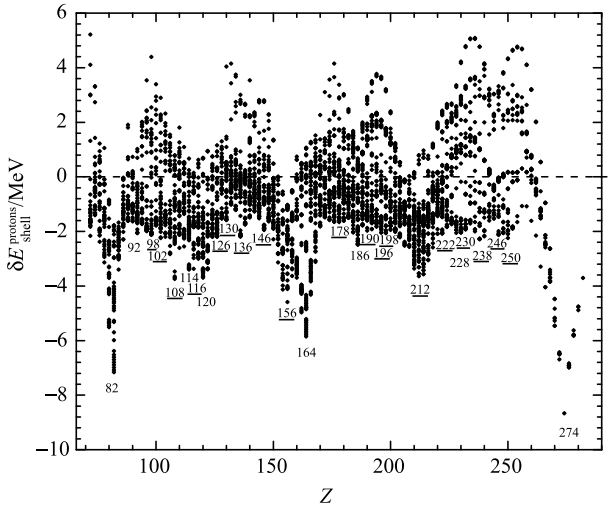

Fig. 1. The proton shell energy correction $\delta E^{\rm protons}_{\rm shell}$ plotted as a function of proton number Z for different isotopes for nuclei with $72 \leqslant Z \leqslant 282$ and $96 \leqslant N \leqslant 540$ that reside in the range between $N_{\rm G}$-10 and two neutron drip-line. The quasi-magic protons are distinguished from the spherical proton magicity by underlined numbers.

Quasi-magic numbers pop up only when nuclear deformations are taken into account, However, the location of magic numbers is not static across the nuclear chart, thus, in identifying nuclear magicity, careful examination of all isotopes and isotones is essential as almost every magic number has an effective range in which the magicity is pronounced and otherwise it disappears and another magic number takes place. This in turn causes some of the magic numbers that are well pronounced in a limited range along the nuclear landscape to appear as small peaks in the accumulative plots. Therefore, in our study, we have performed detailed analysis of the energy plots for all isotopes and isotone in identifying the quasi-magic numbers and the predicted deformed islands of stability. We distinguish quasi-magic protons and neutron numbers from the spherical ones by underlined numbers in the energy plots. The quasi-magic proton numbers, as can be seen from Fig. 1, are signatured at Z = 98, 102, 108, 116, 126, 130, 136, 146, 156, 178, 190, 196, 198, 212, 222, 230, 238, 246 and 250. Besides, the spherical proton magic numbers are signatured at Z = 82, 92, 114, 120, 164, 186, 228 and 274. Furthermore, the proton pairing energy $\delta E^{\rm protons}_{\rm pairing}$ as a function of proton number Z for different isotopes is illustrated in Fig. 2. In Fig. 2, the quasi-magic proton numbers are distinguished by the underlined numbers. The figure shows the presence of Z = 80, 88, 96, 102, 106, 116, 122, 128, 132, 140, 146, 156, 162, 166, 170, 174, 180, 188, 192, 198, 208, 222, 232, 248, 254, 260, 264 and 270 as possible quasi-magic proton numbers. Alongside with the predicted spherical proton magic numbers at Z = 76, 92, 114, 138, 154, 186, 204, 216, 228 and 244.

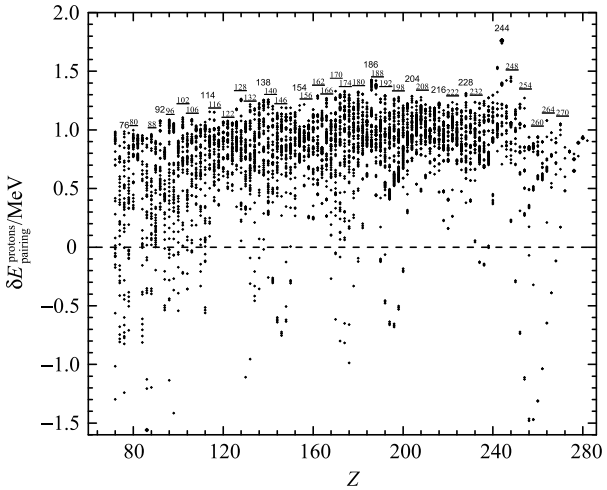

Fig. 2. The proton pairing energy correction $\delta E^{\rm protons}_{\rm pairing}$ plotted as a function of proton number Z for different isotopes for nuclei with $72 \leqslant Z \leqslant 282$ and $96 \leqslant N \leqslant 540$ that reside in the range between $N_{\rm G}$-10 and two neutron drip-line. The quasi-magic proton magicity is distinguished from the spherical proton magicity by underlined numbers.

In the same vein, to investigate the neutron magicity, we explored the dependency of the neutron shell and pairing energies on the neutron number N for even-even nuclei with $72 \leqslant Z \leqslant 282$ and $96 \leqslant N \leqslant 540$ confined between $N_{\rm G}$-10 and two neutron drip-line. Figure 3 reveals the variation of the neutron shell energy $E^{\rm neutrons}_{\rm shell}$ as a function of the neutron number N for different isotones. The plot shows clear evidence for the signature

of the quasi-magic neutron numbers at N = 108, 162, 212, 232, 292, 358, 370, 382 and 464, and faint signatures appeared for possible quasi neutron magicity at N = 108, 158, 248, 264, 440, 446 and 452. Besides, signatures of spherical neutron magic numbers appear at N = 126, 136, 148, 184, 228, 258, 308, 330, 338, 350, 406 and 524. In Fig. 3, the quasi-magic neutron numbers are distinguished by the underlined numbers.

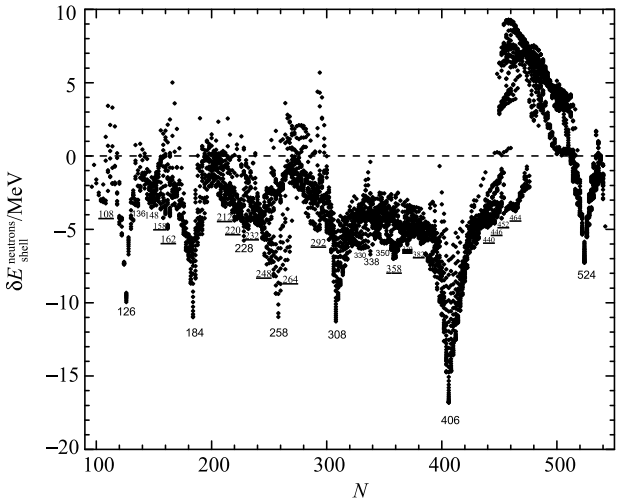

Fig. 3. The neutron shell energy correction $\delta E^{\rm neutrons}_{\rm shell}$ plotted as a function of neutron number N for different isotones for nuclei with 72 $\leqslant Z \leqslant$ 282 and 96 $\leqslant N \leqslant$ 540 that reside in the range between $N_{\rm G}$-10 and two neutron dripline. The neutron quasi magicity is distinguished from the spherical neutron magicity by underlined numbers.

The dependency of the residual pairing correction energy $\delta E^{\rm neutrons}_{\rm pairing}$ on the neutron number N is illustrated in Fig. 4. Signatures of quasi-magic neutron numbers pop up only when the deformations are taken into account and they are distinguished by the underlined numbers in Fig. 4. The neutron numbers N = 108, 120, 152, 162, 172, 192, 220, 232, 238, 244, 252, 282, 290, 294, 302, 322, 342, 352, 358, 366, 370, 376, 400, 416, 446, 450, 498 and 502 show strong evidences of quasi magicity and faint signatures of quasi magicity are found at N= 104, 144, 158, 204, 216, 266, 276, 314, 348, 386, 396, 466, 470, 482, 488 and 508. The other signatures of magicity in Fig. 4 are due to the spherical neutron magic numbers that are pronounced at N = 126, 136, 148, 178, 184, 196, 210, 228, 258, 308, 318, 330, 338, 406 and 432.

Another compelling piece of evidence of neutron magicity can also be inferred from the characterizing features of the shell-plus-pairing correction energy [51, 52]. In Ref. [52], it was found that the shell-plus-pairing correction energy evaluated in the framework of the finite-range droplet model predicts the neutron magicity at N = 126 in polonium isotopes and showed sharp consistency with experimental data obtained using GSI facilities. The use of the shell-plus-pairing correction energy in predicting nuclear magicity was also a success in Ref. [51], as it showed the emergence of the quasi-magic proton number Z = 108, the quasi-magic neutron number N = 162 and the deformed doubly magic nuclei $^{270}108_{162}$ when nuclear deformations were taken into consideration.

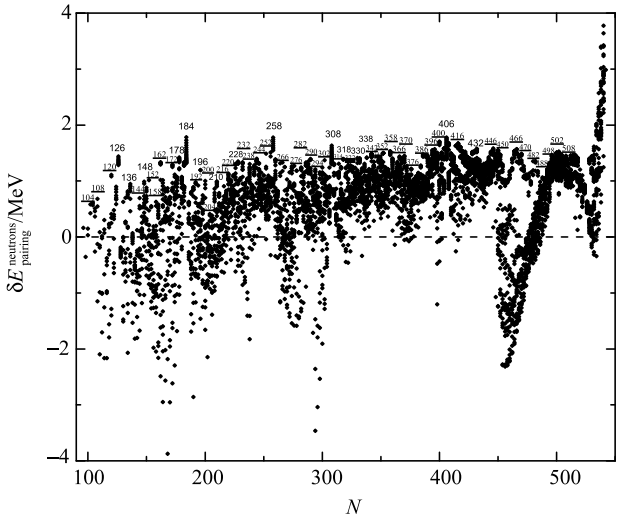

Fig. 4. The neutron pairing energy correction $\delta E^{\rm neutrons}_{\rm pairing}$ plotted as a function of neutron number N for different isotones for nuclei with 72 $\leqslant Z \leqslant$ 282 and 96 $\leqslant N \leqslant$ 540 that reside in the range between $N_{\rm G}$-10 and two neutron dripline. The neutron quasi magicity is distinguished from the spherical neutron magicity by underlined numbers.

In Fig. 5 and Fig. 6, we present the proton shell-plus-pairing energy $\delta E^{\rm protons}_{\rm S+P}$ and the neutron shell-plus-pairing energy $\delta E^{\rm neutrons}_{\rm S+P}$ as a function of the proton number Z for different isotopes and neutron number N for different isotones, respectively. Figure 5 indicates the presence of proton quasi magicity at Z = 96, 108, 116, 130, 136, 146, 156 178, 190, 196, 206, 212, 222, 230, 238, 240 and 250, and spherical proton magicity were pronounced at Z = 82, 92, 114, 120, 164, 186 and 274. On the other hand, Fig. 6 shows the presence of evidences that vary in their strength for neutron quasi magicity at N = 106, 160, 212, 290, 292 and 360 that are indicated by underlined numbers. Besides, the spherical neutron magic numbers are signatured at N = 126, 184, 228, 258, 308, 328, 338, 346, 406 and 524.

In Table 1, we present all the possibly quasi-magic proton numbers that showed a global signature in the proton shell correction energy ($\delta E^{\rm protons}_{\rm shell}$), proton pairing correction energy ($\delta E^{\rm protons}_{\rm pairing}$), proton shell-plus-pairing correction energy ($\delta E^{\rm protons}_{\rm S+P}$) calculations in the range $72 \leqslant Z \leqslant 282$.

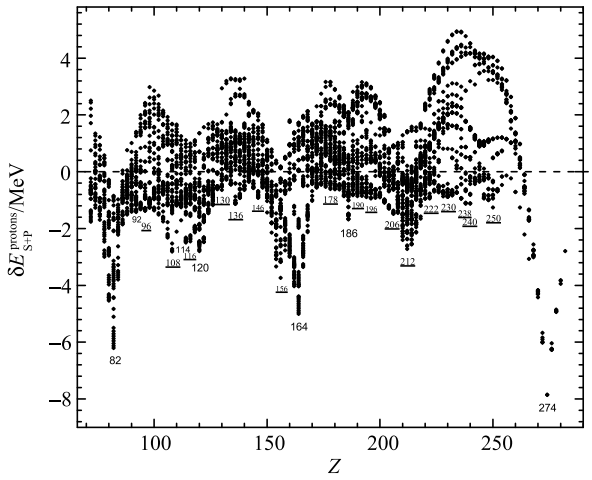

Fig. 5. The proton shell-plus-pairing energy correction $\delta E^{\rm protons}_{\rm S+P}$ plotted as a function of proton number Z for different isotopes for nuclei with $72 \leqslant Z \leqslant 282$ and $96 \leqslant N \leqslant 540$ that reside in the range between $N_{\rm G}$-10 and two neutron drip-line. The proton quasi magicity is distinguished from the spherical proton magicity by underlined numbers.

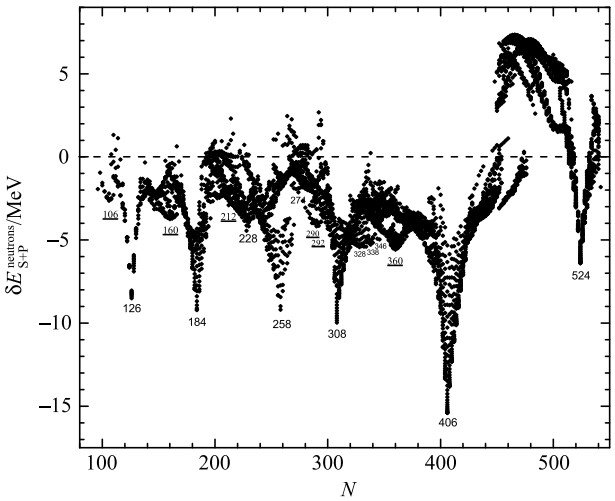

Fig. 6. The neutron shell-plus-pairing energy correction $\delta E^{\rm neutrons}_{\rm S+P}$ plotted as a function of proton number Z for different isotopes for nuclei with $72 \leqslant Z \leqslant 282$ and $96 \leqslant N \leqslant 540$ that reside in the range between $N_{\rm G}$-10 and two neutron drip-line. The neutron quasi magicity is distinguished from the spherical neutron magicity by underlined numbers.

Table 2. The predicted quasi-magic proton numbers (QMPN) based on the proton shell correction enegy ($\delta E^{\rm p}_{\rm S}$), proton pairing correction energy ($\delta E^{\rm p}_{\rm P}$), proton shell-plus-pairing correction energy ($\delta E^{\rm p}_{\rm S+P}$) calculations in the range $72 \leqslant Z \leqslant 282$. For comparisons, we report predictions by other authors namely; Roger A. Rydin [53], J. H. Hamilton et al. [54], H. F. Zhang et al.[55], Yu. Oganessian [56], W. Zhang et al. [31], R. K. Gupta et al. [57], S. Liran et al. [58], D. N. Poenaru et al. [59] , Raj K. Gupta [60], G. Lalasissis [20], P. Möller et al. [15]. ■ indicates the presence of an evidence for proton magicity, □ indicates no evidence for proton magicity, and ☒ indicates that the proton number is not included in the search space in the corresponding reference.

QMPN	$\delta E^{\rm p}_{\rm S}$	$\delta E^{\rm p}_{\rm P}$	$\delta E^{\rm p}_{\rm S+P}$	Ref. [53]	Ref. [54]	Ref. [55]	Ref. [56]	Ref. [31]	Ref. [57]	Ref. [58]	Refs. [59, 60]	Ref. [20]	Ref. [15]
80	□	■	□	☒	☒	☒	☒	☒	■	☒	☒	☒	☒
88	□	■	□	☒	☒	☒	☒	☒	☒	☒	☒	☒	☒
96	□	■	■	□	☒	☒	☒	☒	☒	☒	☒	☒	☒
98	■	□	□	□	☒	☒	☒	☒	☒	☒	☒	☒	☒
102	■	■	□	□	■	□	□	□	☒	□	□	□	□
106	□	■	□	□	□	□	□	■	☒	□	■	■	□
108	■	□	■	■	■	■	■	□	☒	■	■	□	■
116	■	■	■	□	□	□	□	□	☒	■	□	☒	☒
122	□	■	□	□	□	□	□	□	☒	□	□	☒	☒
126	■	■	□	☒	☒	□	☒	■	☒	■	☒	☒	☒
128	□	■	□	☒	☒	□	☒	□	☒	☒	☒	☒	☒
130	■	□	■	☒	☒	☒	☒	□	☒	☒	☒	☒	☒
132	□	■	□	☒	☒	☒	☒	■	☒	☒	☒	☒	☒
136	■	□	■	☒	☒	☒	☒	□	☒	☒	☒	☒	☒
140	□	■	□	☒	☒	☒	☒	□	☒	☒	☒	☒	☒
146	■	■	■	☒	☒	☒	☒	☒	☒	☒	☒	☒	☒
152	□	□	■	☒	☒	☒	☒	☒	☒	☒	☒	☒	☒
156	■	■	■	☒	☒	☒	☒	☒	☒	☒	☒	☒	☒
162	□	■	□	☒	☒	☒	☒	☒	☒	☒	☒	☒	☒
166	□	■	□	☒	☒	☒	☒	☒	☒	☒	☒	☒	☒

Continued

QMPN	$\delta E_{\rm S}^{\rm p}$	$\delta E_{\rm P}^{\rm p}$	$\delta E_{\rm S+P}^{\rm p}$	Ref. [53]	Ref. [54]	Ref. [55]	Ref. [56]	Ref. [31]	Ref. [57]	Ref. [58]	Refs. [59, 60]	Ref. [20]	Ref. [15]
170	□	■	□	⊠	⊠	⊠	⊠	⊠	⊠	⊠	⊠	⊠	⊠
174	□	■	□	⊠	⊠	⊠	⊠	⊠	⊠	⊠	⊠	⊠	⊠
178	■	□	■	⊠	⊠	⊠	⊠	⊠	⊠	⊠	⊠	⊠	⊠
180	□	■	□	⊠	⊠	⊠	⊠	⊠	⊠	⊠	⊠	⊠	⊠
188	□	■	□	⊠	⊠	⊠	⊠	⊠	⊠	⊠	⊠	⊠	⊠
190	■	□	■	⊠	⊠	⊠	⊠	⊠	⊠	⊠	⊠	⊠	⊠
192	□	■	□	⊠	⊠	⊠	⊠	⊠	⊠	⊠	⊠	⊠	⊠
196	■	□	■	⊠	⊠	⊠	⊠	⊠	⊠	⊠	⊠	⊠	⊠
198	■	■	□	⊠	⊠	⊠	⊠	⊠	⊠	⊠	⊠	⊠	⊠
206	□	□	■	⊠	⊠	⊠	⊠	⊠	⊠	⊠	⊠	⊠	⊠
208	□	■	□	⊠	⊠	⊠	⊠	⊠	⊠	⊠	⊠	⊠	⊠
212	■	□	■	⊠	⊠	⊠	⊠	⊠	⊠	⊠	⊠	⊠	⊠
222	■	■	■	⊠	⊠	⊠	⊠	⊠	⊠	⊠	⊠	⊠	⊠
230	■	□	■	⊠	⊠	⊠	⊠	⊠	⊠	⊠	⊠	⊠	⊠
232	□	■	□	⊠	⊠	⊠	⊠	⊠	⊠	⊠	⊠	⊠	⊠
238	■	□	■	⊠	⊠	⊠	⊠	⊠	⊠	⊠	⊠	⊠	⊠
240	□	□	■	⊠	⊠	⊠	⊠	⊠	⊠	⊠	⊠	⊠	⊠
246	■	□	□	⊠	⊠	⊠	⊠	⊠	⊠	⊠	⊠	⊠	⊠
248	□	■	□	⊠	⊠	⊠	⊠	⊠	⊠	⊠	⊠	⊠	⊠
250	■	□	■	⊠	⊠	⊠	⊠	⊠	⊠	⊠	⊠	⊠	⊠
254	□	■	□	⊠	⊠	⊠	⊠	⊠	⊠	⊠	⊠	⊠	⊠
260	□	■	□	⊠	⊠	⊠	⊠	⊠	⊠	⊠	⊠	⊠	⊠
264	□	■	□	⊠	⊠	⊠	⊠	⊠	⊠	⊠	⊠	⊠	⊠
270	□	■	□	⊠	⊠	⊠	⊠	⊠	⊠	⊠	⊠	⊠	⊠

Systematic investigations assessing the stability of nuclei, in the range of superheavy nuclei, have been introduced in many recent publications. In Ref. [65], Staszczak et al. carried out a systematic self-consistent study in Skyrme-Hartree-Fock-Bogoliubov approach, and shed the light on the center of enhanced stability for even-even nuclei in the range $108 \leqslant Z \leqslant 126$ and $148 \leqslant N \leqslant 188$. Also in Ref. [66], Dobaczewski et al. explored the ground and excited state properties of nuclei with $92 \leqslant Z \leqslant 104$ and $144 \leqslant N \leqslant 156$ using three energy density functional (EDF) approaches based on covariant, Skyrme, and Gogny functionals. Dobaczewski et al found significant differences between the results obtained within these different EDFs. None of the studied global EDF parameterisations was found to precisely reproduce the variations of the shell structure observed in experiments. Arguably, this can be due to small deficiencies of the resulted deformed shell properties [66]. Furthermore, Agbemava et al. introduced a systematic study using five types of covariant energy density functionals (NL3*, DD-ME2, and PC-PK1) for even-even nuclei spanning the range of superheavy nuclei with $100 \leqslant Z \leqslant 130$ and neutron number confined beteen the proton drip-line and N=196 [67]. Their study showed that the neutron shell gap at $N = 172$ has a very limited impact in the Z-N space with the deformation is taken into account, a result that is confirmed by all the used functionals. On the other hand, the impact of the proton shell gap at $Z = 120$ and neutron shell gap at $N = 184$ strongly depend on the functional, in which it completely disappears in DD-PC1 and DD-MEδ. So, systematic studies in the region of superheavy nuclei are of great interest, Nevertheless, the experimental results are yet the deciding tool that will help to drastically reduce the number of models and parameterizations and help us understand the yet mysterious nuclear systems.

The exact positions of the magic numbers that appear only when deformations are taken into account are of great importance, and there are many studies in which quasi-magic numbers are the main topic. In assessing the results presented here, in Table 2, we illustrate the quasi-magic proton numbers predicted in Refs. [15, 20, 31, 53–60] together with our predictions. It is important to note that in some of these references quasi-magic numbers is not the only focus of their work, hence in some of the references they considered a narrow search space. The same comparison for the case of quasi-magic neutron numbers is illustrated in Table 3.

In this study we have accessed regions of the N-Z space that have not been explored before, especially in the heaviest systems. In their recent paper [31], W. Zhang et al. performed a rigorous study using the relativistic continuum Hartree-Bogoliubov (RCHB) theory with interactions NL1, NL3, NLSH, TM1, TW99, DD-ME1, PK1, and PK1R for nuclei with Z=100-140 and neutron numbers dominate the range $N = (Z + 30) - (2Z + 32)$. W. Zhang et al used the calculations of the two-nucleon separation energies, the two-nucleon gaps, the shell correction energies, the pairing energies, and the pairing gaps for studying proton and neutron magicity. Z = 106, 126 and 132 and N = 172, 216 and 252 are the reported proton and neutron magic numbers that appear due to deformations. However, as can be seen in Table 2 and Table 3, our analysis reproduced the same result and showed that Z = 102, 108, 116, 122, 128, 130, 136 and 140 and N= 144, 152, 158, 160, 162, 192, 200, 204, 212, 220, 232, 244, 248, 264, 266, 276, 282, 290, 292, 294, 302 are additional proton and neutron magic numbers that appear only when deformations are taken into account. Arguably, these differences are due to the shifts of nuclear magicity along the nuclear landscape, as every magic number has a range in which the magicity prevails, however, it disappears otherwise and another magic number takes over.

Despite the appearance of global signatures of quasi-magic proton and quasi-magic neutron numbers that are observed in the shell and pairing correction energy calculations illustrated in the previous figures, deeper analysis shows the presence of quasi-magic proton and quasi-magic neutron numbers that show remarkable local evidences for magicity, and contribute to the formation of islands of stability with no global signatures in the energy calculations. Furthermore, the quasi-magic numbers are found to be not static across the search space landscape and shifts in nuclear magicity are found for both quasi-magic proton and neutron numbers, a behavior that characterizes nuclear magicity and adds to the mystery of nuclear systems.

Doubly magic nuclei are exceptionally stable systems. Thus, it is important to examine the exact positions of the possible doubly magic nuclei. Evidently, not all possible combinations of the predicted proton and neutron magic numbers are necessarily deformed doubly magic nuclei. In fact, some of these combinations are not in the center of a stability valley. Among all possible combinations of proton and neutron magic numbers only 133 nuclei are proved to be located at the centers of islands of stability, of which some deformed doubly magic nuclei have been extensively investigated, for instance $^{270}108_{162}$, and others are being reported for the first time.

Table 3. The predicted quasi-magic neutron numbers (QMNN) based on the neutron shell enegy ($\delta E^{\rm n}_{\rm S}$), neutron residual pairing energy ($\delta E^{\rm n}_{\rm P}$), neutron shell-plus-pairing correction energy ($\delta E^{\rm n}_{\rm S+P}$) calculations in the range $72 \leqslant Z \leqslant 282$. For comparisons, we report predictions by other authors namely; Roger A. Rydin [53], J. H. Hamilton et al. [54], H. F. Zhang et al.[55], Yu. Oganessian [56], W. Zhang et al. [31], R. K. Gupta et al. [57], S. Liran et al. [58], D. N. Poenaru et al. [59] , Raj K. Gupta [60], G. Lalazissis [20], P. Möller et al. [15]. ■ indicates the presence of an evidence for neutron magicity, □ indicates no evidence for neutron magicity, and ⊠ indicates that the neutron number is not included in the search space in the corresponding reference.

QMNN	$\delta E^{\rm n}_{\rm S}$	$\delta E^{\rm n}_{\rm P}$	$\delta E^{\rm n}_{\rm S+P}$	Ref. [15]	Ref. [20]	Ref. [64]	Ref. [53]	Ref. [54]	Ref. [55]	Ref. [56]	Ref. [31]	Ref. [57]	Refs. [59, 60]
104	□	■	□	⊠	⊠	⊠	⊠	⊠	⊠	■	⊠	⊠	⊠
106	□	□	■	⊠	⊠	⊠	⊠	⊠	⊠	⊠	⊠	⊠	⊠
108	■	■	□	⊠	⊠	⊠	⊠	⊠	⊠	⊠	■	⊠	⊠
120	□	■	□	⊠	⊠	⊠	⊠	⊠	⊠	⊠	□	⊠	⊠
144	□	■	□	□	⊠	□	⊠	⊠	□	⊠	□	⊠	□
152	□	■	□	□	■	□	■	□	□	⊠	■	⊠	■
158	■	■	□	■	□	□	□	□	□	⊠	□	□	□
160	□	□	■	□	□	□	□	■	□	⊠	□	■	□
162	■	■	□	□	■	■	■	■	□	⊠	■	□	■
172	□	■	□	■	□	□	□	■	■	⊠	■	□	⊠
192	□	■	□	⊠	⊠	□	⊠	⊠	□	⊠	□	⊠	⊠
200	□	■	□	⊠	⊠	⊠	⊠	⊠	□	⊠	⊠	⊠	⊠
204	□	■	□	⊠	⊠	⊠	⊠	⊠	□	⊠	⊠	⊠	⊠
212	■	□	■	⊠	⊠	⊠	⊠	⊠	□	⊠	⊠	⊠	⊠
216	□	■	□	⊠	⊠	⊠	⊠	⊠	■	⊠	⊠	⊠	⊠
220	■	■	□	⊠	⊠	⊠	⊠	⊠	□	⊠	⊠	⊠	⊠
232	■	■	□	⊠	⊠	⊠	⊠	⊠	□	⊠	⊠	⊠	⊠
238	□	■	□	⊠	⊠	⊠	⊠	⊠	■	⊠	⊠	⊠	⊠

Continued

QMNN	$\delta E^{\rm n}_{\rm S}$	$\delta E^{\rm n}_{\rm P}$	$\delta E^{\rm n}_{\rm S+P}$	Ref. [15]	Ref. [20]	Ref. [64]	Ref. [53]	Ref. [54]	Ref. [55]	Ref. [56]	Ref. [31]	Ref. [57]	Refs. [59, 60]
244	□	■	□	⊠	⊠	⊠	⊠	⊠	□	⊠	⊠	⊠	⊠
248	■	□	□	⊠	⊠	⊠	⊠	⊠	□	⊠	⊠	⊠	⊠
252	□	■	□	⊠	⊠	⊠	⊠	⊠	■	⊠	⊠	⊠	⊠
264	■	□	□	⊠	⊠	⊠	⊠	⊠	□	⊠	⊠	⊠	⊠
266	□	■	□	⊠	⊠	⊠	⊠	⊠	□	⊠	⊠	⊠	⊠
276	□	■	□	⊠	⊠	⊠	⊠	⊠	□	⊠	⊠	⊠	⊠
282	□	■	□	⊠	⊠	⊠	⊠	⊠	□	⊠	⊠	⊠	⊠
290	□	■	■	⊠	⊠	⊠	⊠	⊠	□	⊠	⊠	⊠	⊠
292	■	□	■	⊠	⊠	⊠	⊠	⊠	□	⊠	⊠	⊠	⊠
294	□	■	□	⊠	⊠	⊠	⊠	⊠	□	⊠	⊠	⊠	⊠
302	□	■	□	⊠	⊠	⊠	⊠	⊠	□	⊠	⊠	⊠	⊠
314	□	■	□	⊠	⊠	⊠	⊠	⊠	⊠	⊠	⊠	⊠	⊠
322	□	■	□	⊠	⊠	⊠	⊠	⊠	⊠	⊠	⊠	⊠	⊠
342	□	■	□	⊠	⊠	⊠	⊠	⊠	⊠	⊠	⊠	⊠	⊠
348	□	■	□	⊠	⊠	⊠	⊠	⊠	⊠	⊠	⊠	⊠	⊠
352	□	■	□	⊠	⊠	⊠	⊠	⊠	⊠	⊠	⊠	⊠	⊠
358	■	■	□	⊠	⊠	⊠	⊠	⊠	⊠	⊠	⊠	⊠	⊠
360	□	□	■	⊠	⊠	⊠	⊠	⊠	⊠	⊠	⊠	⊠	⊠
366	□	■	□	⊠	⊠	⊠	⊠	⊠	⊠	⊠	⊠	⊠	⊠
370	■	■	□	⊠	⊠	⊠	⊠	⊠	⊠	⊠	⊠	⊠	⊠
376	□	■	□	⊠	⊠	⊠	⊠	⊠	⊠	⊠	⊠	⊠	⊠
382	■	□	□	⊠	⊠	⊠	⊠	⊠	⊠	⊠	⊠	⊠	⊠
386	□	■	□	⊠	⊠	⊠	⊠	⊠	⊠	⊠	⊠	⊠	⊠
396	□	■	□	⊠	⊠	⊠	⊠	⊠	⊠	⊠	⊠	⊠	⊠
400	□	■	□	⊠	⊠	⊠	⊠	⊠	⊠	⊠	⊠	⊠	⊠
416	□	■	□	⊠	⊠	⊠	⊠	⊠	⊠	⊠	⊠	⊠	⊠
440	■	□	□	⊠	⊠	⊠	⊠	⊠	⊠	⊠	⊠	⊠	⊠
446	■	■	□	⊠	⊠	⊠	⊠	⊠	⊠	⊠	⊠	⊠	⊠
450	□	■	□	⊠	⊠	⊠	⊠	⊠	⊠	⊠	⊠	⊠	⊠
452	■	□	□	⊠	⊠	⊠	⊠	⊠	⊠	⊠	⊠	⊠	⊠
464	■	□	□	⊠	⊠	⊠	⊠	⊠	⊠	⊠	⊠	⊠	⊠
466	□	■	□	⊠	⊠	⊠	⊠	⊠	⊠	⊠	⊠	⊠	⊠
470	□	■	□	⊠	⊠	⊠	⊠	⊠	⊠	⊠	⊠	⊠	⊠
482	□	■	□	⊠	⊠	⊠	⊠	⊠	⊠	⊠	⊠	⊠	⊠
498	□	■	□	⊠	⊠	⊠	⊠	⊠	⊠	⊠	⊠	⊠	⊠
502	□	■	□	⊠	⊠	⊠	⊠	⊠	⊠	⊠	⊠	⊠	⊠
508	□	■	□	⊠	⊠	⊠	⊠	⊠	⊠	⊠	⊠	⊠	⊠

For a more concise illustration, in Fig. 7, we represent the resulting quasi-magic proton and quasi-magic neutron numbers by horizontal and vertical lines, respectively. The solid horizontal lines indicate proton magic numbers that show local evidence for magicity in both shell and pairing correction energy calculations, dashed lines indicates quasi-magic numbers that locally show a magicity sign only in the pairing calculations, dotted lines denote quasi-magic proton numbers that show signatures only in the shell calculations and dash dotted lines represent quasi-magic proton numbers that show local faint signatures for magicity in the calculations and are not well pronounced in the shell and pairing plots. The predicted doubly magic nuclei located at the center of an island of stability which has quasi-magic proton and neutron numbers are represented by different points in Fig. 7 depending on their depth, strength of evidence and location between N_G-10 and two neutron drip line. The doubly magic nuclei are connected in such a way that shifts in nuclear magicity can easily be inferred from the plot.

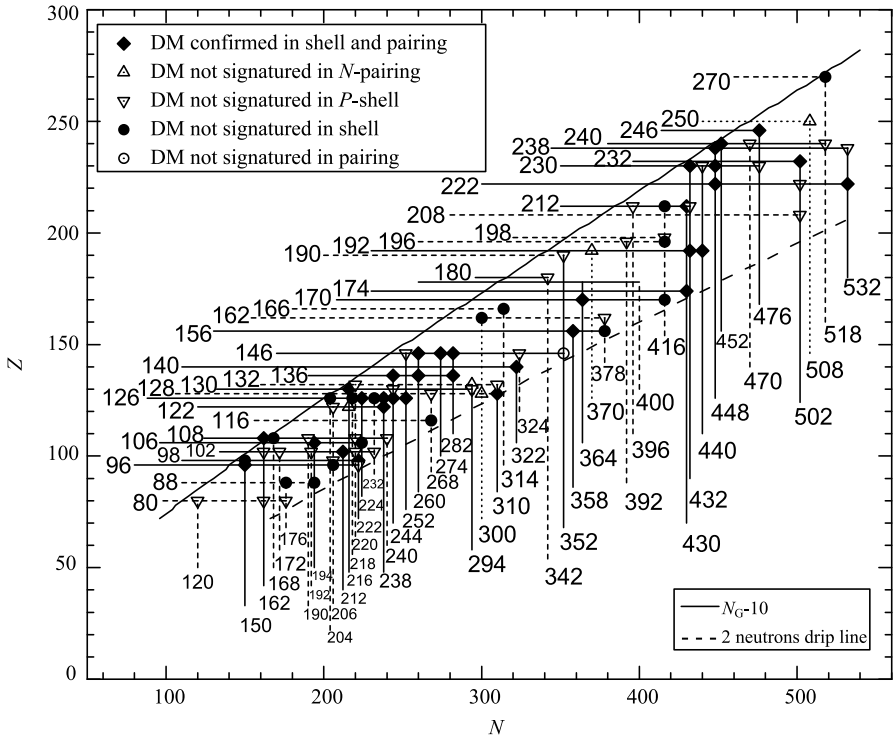

Fig. 7. The predicted doubly magic nuclei located at the center of an island of stability which has quasi-magic proton and neutron numbers in the N-Z plane in the range $72 \leqslant Z \leqslant 282$ and $96 \leqslant N \leqslant 540$ for nuclei confined between $N_{\rm G}$-10 (bold solid line) and two neutron drip-line (bold dashed line).

Although quasi magicity is generally less pronounced compared to spherical magicity, there are some quasi-magic numbers that show predominance and take over spherical magic numbers when deformations are taken into considerations. For instance, the proton quasi magicity at $Z = 126$ dominates the neutron range $N =$ 204–252, and it is more pronounced takes than the spherical proton magicity at $Z = 124$ that shows magicity close to the two neutrons drip line around $N = 264$, where the proton quasi magicity at Z disappears. Furthermore, when deformation is taken into account the proton quasi magicity at $Z = 80$ becomes as pronounced as the strong spherical proton magicity at $Z = 82$ in the ranges around N= 120, 136, 162 and 176, especially in the residual pairing energy calculations.

In Fig. 8, we present the predicted doubly magic nuclei located at the center of an island of stability which has quasi-magic proton and spherical neutron magic numbers. As can be seen from the figure, the quasi magicity at $Z = 108$ spans the neutron range $N = 240 - 260$ around the two neutron drip line. However, the quasi magicity at $Z = 106$ shows strength only around the spherical neutron magic number $N =$ 184 and it disappears otherwise. Furthermore, no clear pattern for the islands of stability can be inferred, as both the spherical and quasi magicity disappear with increasing both protons and neutrons. For instance, the spherical magicity at $N = 432$ shows significance at the quasi-magic proton numbers $Z = 192$, 212 and 230, and the spherical magicity at $N = 522$ shows magicity only around $Z = 232$ and otherwise shows no evidence.

In Fig. 9 we illustrate the predicted doubly magic nuclei that only have quasi-magic neutron numbers. Close to the two neutron drip line the spherical proton magicity $Z = 92$ shows strong presence at the quasi-magic neutron numbers $N = 204$ and 212, and interestingly the neutron quasi magicity at $N = 204$ and 212 is volatile close to higher proton numbers and the magicity at N = 200 and 206 takes over effectively around $Z = 120$, forming deep islands of stability. Moreover, it is only the spherical proton magicity at $Z = 154$ that shows predominance along the search space in both ranges close to the stability line and the two neutron drip line. However its magicity disappears at the quasi-magic neutron numbers in the neutron range $N = 332 - 364$. Again no clear pattern for these islands of stability can be inferred from these results. These results are in line with what was found in Ref. [9] for spherical shell stability. The shifts in the initial pattern of the islands of stability for both quasi and spherical magicity, especially in the super and hyperheavy regions, can be argued due to the presence of large single-particle level density and also the appearance of many low-j shells around the Fermi level [9].

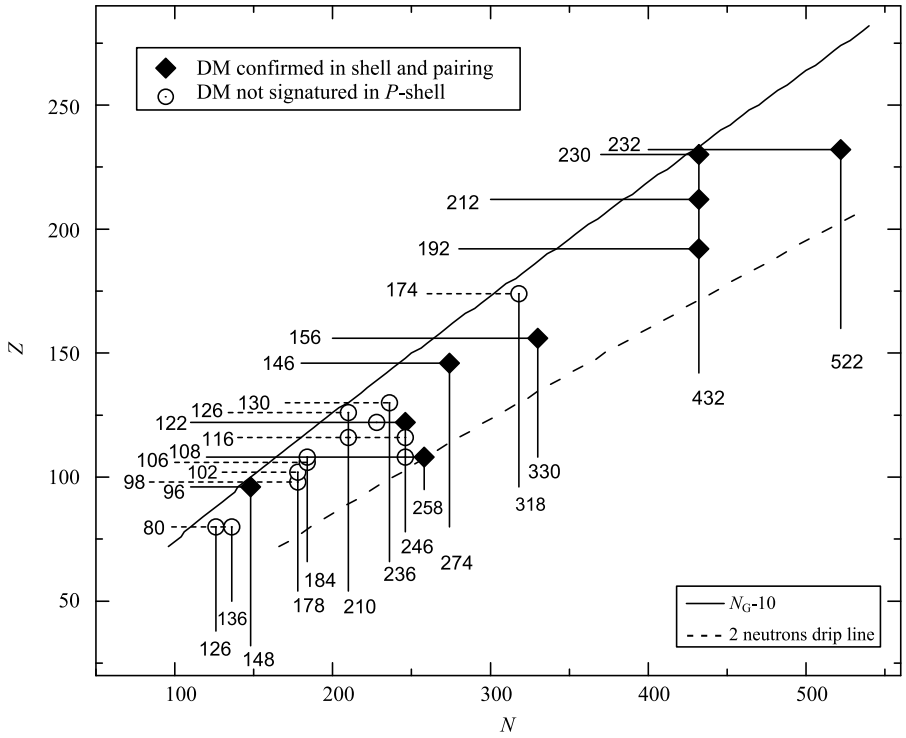

Fig. 8. The predicted doubly magic nuclei located at the center of an island of stability with quasi-magic proton and spherical neutron magic numbers in the N-Z plane in the range $72 \leqslant Z \leqslant 282$ and $96 \leqslant N \leqslant 540$ for nuclei confined between $N_{\rm G}$-10 (bold solid line) and two neutrons drip-line (bold dashed line).

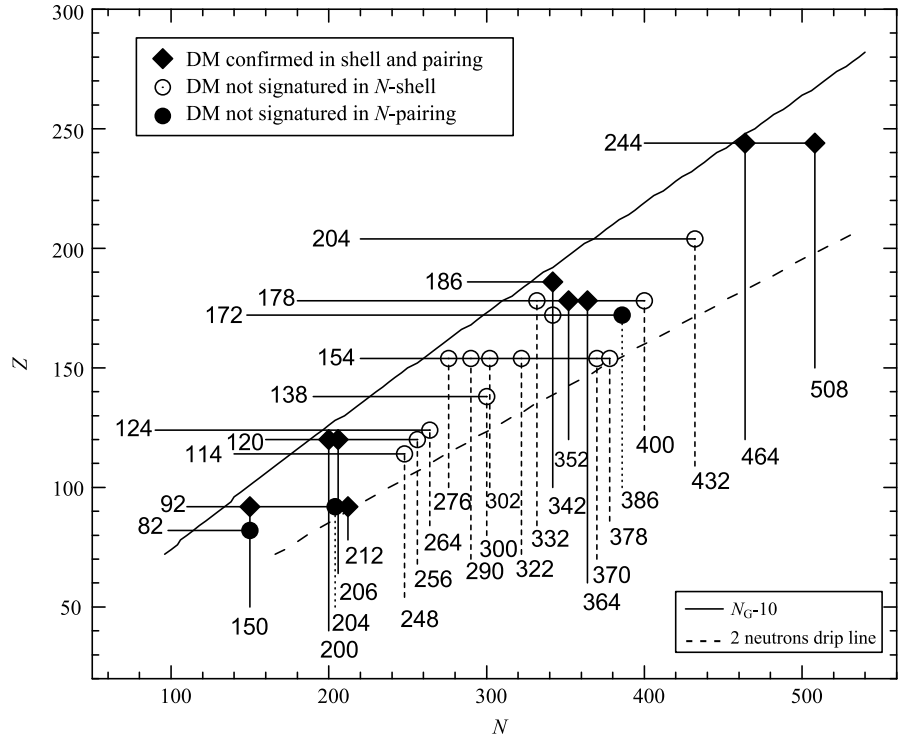

Fig. 9. The predicted doubly magic nuclei located at the center of an island of stability with only quasi-magic neutron numbers in the N-Z plane in the range $72 \leqslant Z \leqslant 282$ and $96 \leqslant N \leqslant 540$ for nuclei confined between $N_{\rm G}$-10 (bold solid line) and two neutron drip-line (bold dashed line).

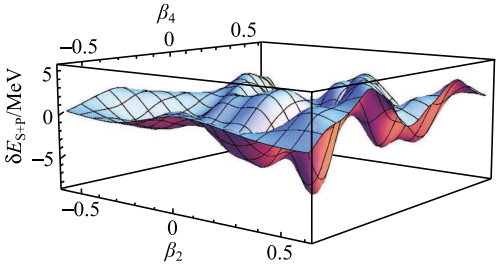

(a) 3D shell-plus-pairing energy surface of the nucleus $^{270}Hs_{162}$ plotted as a function of quadrupole and hexadecapole deformations. The global minimum is located at (0.24, –0.1, –8.53 MeV).

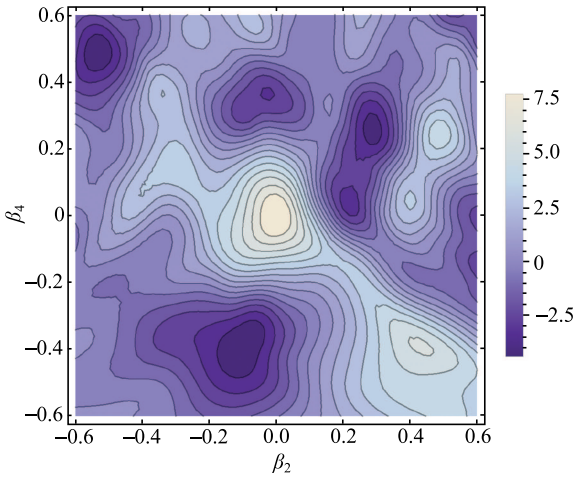

(b) A contour map of the shell-plus-pairing energy of the nucleus $^{314}No_{212}$ projected on the (β_2, β_4) plane at β_3=0 and β_6=0. The globle minimum is located at (–0.54, 0.48) coordinate and has a value of –4.42 MeV. The separation energy between contour lines is 0.81 MeV.

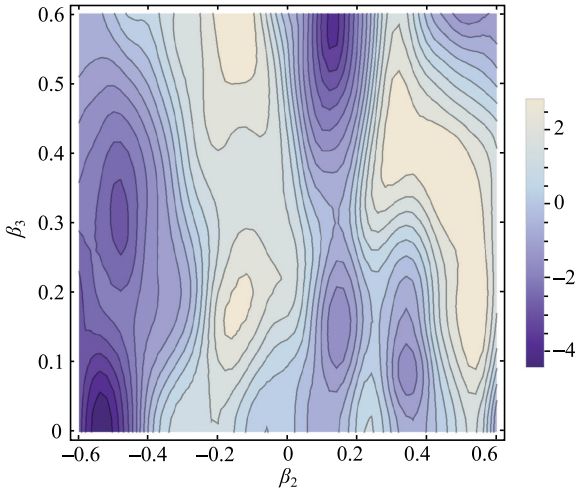

(c) A contour map of the shell-plus-pairing energy of the nucleus $^{314}No_{212}$ plotted as a function of quadrupole and octupole deformations at β_4=0.48 and β_6=0.The globle minimum is located at (–0.54, 0.00) coordinate and has a value of –4.42 MeV. The separationenergy between contour lines is 0.48 MeV.

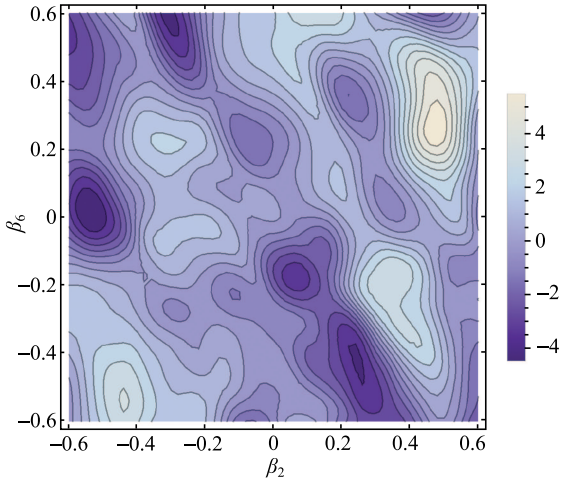

(d) A contour map of the shell-plus-pairing energy of the nucleus $^{314}No_{212}$ plotted as a function of quadrupole and hexacontatetrapole deformations at β_3 = 0.00 and β_4 = 0.48. The globle minimum is located at (–0.54, 0.02) coordinate and has a value of –4.48 MeV. The separation energy between contour lines is 0.66 MeV.

Fig. 10. (color online) As an example, (a) 3D plot of the shell-plus-pairing energy of the $^{270}Hs_{162}$ nucleus as function of (β_2, β_4) deformation space, and the behavior of the shell-plus-pairing energy δE_{S+P} of the predicted deformed doubly magic nucleus $^{314}No_{212}$ in (b) (β_2, β_4), (c) (β_2, β_3) and (d) (β_2, β_6) deformation spaces.

Yet another important aspect of the reported nucleon magic numbers is that some spherical/quasi proton (neutron) magic numbers show plausible signatures for being possible spherical/quasi neutron (proton) magic numbers. For instance, spherical proton magicity is observed at $Z = 274$ and it dominates the neutron range around the stability line. However, faint evidence for spherical magicity is observed at $N = 274$, which is effective only around $Z = 114$, which is very close to the two neutron drip line. Furthermore, the nucleus $^{388}114_{274}$ showed shape coexistence, and being spherical in the ground state is not the predominant preference. On the other hand, $N = 126$ shows strong evidence in both the shell and pairing energy calculations for being a spherical neutron magic number, and its magicity paid off in forming the exceptionally stable island centered at $^{208}Pb_{126}$. Nevertheless, we found no evidence for spherical magicity at $Z = 126$, and only when nuclear deformations are

taken into account does the magicity evidence at $Z = 126$ appear, forming relatively deep islands of stability among which are the ones centered at the deformed nuclei $^{330}126_{204}$ and $^{378}126_{252}$. Furthermore, $Z = 120$, 172, 204, 244 are found to be spherical proton numbers, while $N = 120$, 172, 204 and 244 are found to have quasi magicity. However, $N = 126$, 136, 170, 196, 246 and 250 are found to be spherical proton magic numbers, while $Z = 126$, 136, 170, 196, 246 and 250 are found to possess proton quasi magicity. Furthermore, protons and neutrons are both found to exhibit quasi magicity at Z, $N = 162$, 190, 192, 212, 222, 232, 238 and 240, and both are found to exhibit spherical magicity at Z, $N = 114$, 178, 210, 228 and 274, in which they vary in both the strength of evidence of nuclear magicity and the effective range along the nuclear landscape through which the nucleon magicity is significant.

The neutron number N=172 strongly emerges as a possible magic number for neutrons only when deformations are taken into consideration, and it contributes to the formation of the deformed doubly magic nucleus $^{274}\mathrm{No}_{172}$. In the range between $N = 150 - 190$, only $N = 164$, 178 and 184 show strong evidence for spherical magicity, and a faint local signature is seen for $N = 170$ around $Z = 82$. Furthermore, even with the presence of the deep, well established proton spherical magic number at Z=82, our calculations show that the nucleus $^{254}\mathrm{Pb}_{172}$ is slightly shifted from being spherical in the ground state. Moreover, we found that among all $N = 172$ isotones in the range $Z = 74 - 112$ the nucleus $^{252}\mathrm{Hg}_{172}$ shows plausible evidence for being a deformed doubly magic nucleus. However, interestingly, the neutron $N = 172$ was reported to have spherical magicity (see for example [61] and references therein) especially around $Z = 120$, as Sil et al. showed that $^{292}120_{172}$ is a spherical doubly magic nucleus. Into the bargain, extensive studies on nuclear magic numbers using different models showed variations in the prediction of shell closures, and many reports suggested that the nuclear magicity depends on both model and force type.

The reliability of the pairing energy calculations in predicting nucleon magicity is remarkable in our calculations. For instance, the neutron shell calculations show no global signature for neutron magicity at N=244, but strong evidence is present in the global pairing energy calculations indicating $N = 244$ as a possible neutron magic number. Further investigations proved that the 244 isotones, $^{370}126_{244}$, $^{374}130_{244}$, $^{380}136_{244}$, are deformed doubly magic nuclei and show local signatures in both pairing and shell correction energies in the proton range between $Z = 126$ and 136. On the other hand, the shell correction energy also shows remarkable reliability in predicting the nucleon magicity. For example, the proton magicity at $Z = 136$ is not signatured globally in the residual pairing energy calculations, and a strong signature is present for $Z = 136$. With further detailed investigations we found that the isotopes $^{380}136_{244}$, $^{396}136_{260}$, $^{418}136_{282}$ are deformed doubly magic nuclei and their magicity are signatured with local evidence in both shell and residual pairing correction energy.

In assessing the structural properties of the predicted doubly magic nuclei, the behavior of the shell-plus-pairing energy surfaces is examined as a function of four axially-symmetric deformation parameters representing quadrupole (β_2), octupole (β_3), hexadecapole (β_4) and hexacontatetrapole (β_6) deformations. As an example of the behavior of shell-plus-pairing correction energy surface in (β_2, β_4) deformation space, in Fig. 10(a) the 3D surface of $\delta E_{\mathrm{S+P}}$ of the predicted deformed doubly magic nucleus $^{270}\mathrm{Hs}_{162}$ as a function of β_2 and β_4 deformation parameters is illustrated. As indicated in the figure, the global minimum has a value of -8.53 MeV, and is located at (β_2, β_4) = (0.24, -0.1). In estimating the ground state deformation preference of the predicted doubly magic nuclei, we used the values of β_4 that correspond to the global minimum of the macroscopic energy in (β_2, β_4) space in producing the energy surface in (β_2, β_3) space. Then we used the values of β_3 that correspond to the global minimum in (β_2, β_3) space in producing the energy surface in (β_2, β_6) space. As an illustrative example, in Fig. 10(b) we present the informative plot, a contour map of the $\delta E_{\mathrm{S+P}}$ energy of $^{314}\mathrm{No}_{212}$ nucleus projected on the plane (β_2, β_4) at $\beta_3 = \beta_6 = 0.00$. In producing the contour map of Fig. 10(b), we used 15 contour lines with energy separation of 0.81 MeV between the contour lines. The $\delta E_{\mathrm{S+P}}$ energy surface shows a strong presence of a deep global minimum in the β_2 and β_4 space located at (β_2, β_4)=(-0.54, 0.48) with energy of -4.42 MeV. The shell and pairing correction energies are insensitive to the sign of the β_3 deformation parameter, therefore we only consider positive values for β_3 deformation parameter. In Fig. 10(c), we present a contour map of the $\delta E_{\mathrm{S+P}}$ energy of $^{314}\mathrm{No}_{212}$ nucleus projected on the plane (β_2, β_3) at $\beta_4 = 0.48$ and $\beta_6 = 0.00$. The contour map of Fig. 10(c) was produced using 15 contour lines with energy separation of 0.48 MeV between the contour lines. Clearly, the $^{314}\mathrm{No}_{212}$ doubly magic nucleus shows a strong preference of being non-spherical at the ground state. The global minimum of the shell-plus-pairing correction energy in the (β_2, β_3) deformation space reads -4.42 MeV and is located at (β_2, β_3) = (-0.54, 0.00). Furthermore, n Fig. 10(d), a contour map of the $\delta E_{\mathrm{S+P}}$ energy of $^{314}\mathrm{No}_{212}$ nucleus projected on the plane (β_2, β_6) at $\beta_3 = 0.00$ and $\beta_4 = 0.48$ is presented. As indicated in Fig. 10(d), the global minimum is located at (β_2, β_6) = (-0.54, 0.02) at $\delta E_{\mathrm{S+P}}$ =-0.48 MeV. Likewise, exploration is carried out for all the predicted doubly magic nuclei.

In Table 4, we report the predicted ground state characteristics of all the resulted doubly magic nuclei located at the center of an island of stability possessing quasi-magic proton and neutron numbers. We categorize the proposed doubly magic nuclei into five groups. Group 1, indicated by "♦", represents the proposed doubly magic nuclei that are located in the center of locally deep islands of stability with magicity signatures witnessed in both the shell and pairing energy calculations, namely; $^{246}Cm_{150}$, $^{320}Cf_{222}$, $^{314}No_{212}$, $^{300}Sg_{194}$, $^{270}Hs_{162}$, $^{360}122_{238}$, $^{350}126_{224}$, $^{364}126_{238}$, $^{370}126_{244}$, $^{378}126_{252}$, $^{438}128_{310}$, $^{346}130_{216}$, $^{380}136_{244}$, $^{418}136_{282}$, $^{462}140_{322}$, $^{396}136_{260}$, $^{406}146_{260}$, $^{428}146_{282}$, $^{514}156_{358}$, $^{534}170_{364}$, $^{604}174_{430}$, $^{624}192_{432}$, $^{632}192_{440}$, $^{642}212_{430}$, $^{670}222_{448}$, $^{754}222_{532}$, $^{662}230_{432}$, $^{678}230_{448}$, $^{734}232_{502}$, $^{686}238_{448}$, $^{692}240_{452}$, $^{722}246_{476}$. Group 2, indicated by "●", represents double nuclei that are found to be at the centers of islands of stability with magicity signatures witnessed in only the pairing energy calculations, namely; $^{264}Ra_{176}$, $^{282}Ra_{194}$, $^{302}Cm_{206}$, $^{248}Cf_{150}$, $^{330}Sg_{224}$, $^{276}Hs_{168}$, $^{384}116_{268}$, $^{330}126_{204}$, $^{344}126_{218}$, $^{358}126_{232}$, $^{534}156_{378}$, $^{462}162_{300}$, $^{480}166_{314}$, $^{586}170_{416}$, $^{612}196_{416}$, $^{628}212_{416}$, $^{788}270_{518}$. Group 3, indicated by "○", are predicted double nuclei that are found to be at the centers of islands of stability with magicity signatures witnessed in only the shell energy calculations, namely; $^{498}146_{352}$. The fourth group indicated by "▽" contains doubly magic nuclei that are either not signatured in the neutron pairing calculations as for $^{338}122_{216}$, $^{428}128_{300}$, $^{562}192_{370}$, $^{758}250_{508}$, or not signatured in the proton pairing energy calculations as for $^{426}132_{294}$. Group 5, indicated by "△", represents doubly magic nuclei in which the proton magicity shows signatures only in the pairing energy calculations as for $^{200}Hg_{120}$, $^{242}Hg_{162}$, $^{256}Hg_{176}$, $^{318}Cm_{222}$, $^{274}No_{172}$, $^{322}No_{220}$, $^{334}No_{232}$, $^{264}No_{162}$, $^{298}Hs_{190}$, $^{348}Hs_{240}$, $^{328}122_{206}$ $^{396}128_{268}$, $^{424}130_{294}$, $^{374}130_{244}$, $^{442}132_{310}$, $^{398}146_{252}$, $^{470}146_{324}$, $^{540}162_{378}$, $^{522}180_{342}$, $^{588}196_{392}$, $^{710}208_{502}$, $^{724}222_{502}$, $^{706}230_{476}$, or the neutron magicity showed signatures only in the pairing energy calculations as for $^{304}Cf_{206}$, $^{294}No_{192}$, $^{328}Hs_{220}$, $^{352}132_{220}$, $^{542}190_{352}$, $^{614}198_{416}$, $^{608}212_{396}$, $^{644}212_{432}$, $^{670}230_{440}$, $^{770}238_{532}$, $^{710}240_{470}$, $^{758}240_{518}$.

Table 4. The neutron shell ($\delta E_{\rm S}^{\rm n}$), proton shell ($\delta E_{\rm S}^{\rm p}$), neutron pairing ($\delta E_{\rm P}^{\rm n}$), proton pairing ($\delta E_{\rm P}^{\rm p}$), the sum of proton and neutron shell-plus-pairing energy corrections ($\delta E_{\rm S+P}$) and the calculated quadrupole β_2, octupole β_3, hexadecapole β_4 and hexacontatetrapole β_6 deformations for the predicted doubly magic nuclei. Detailed explanation of the different types of the doubly magic nuclei indicated below by the symbols ♦, ●, ○ △ and ▽ are explained in detail in the text.

Z	N	A	type	β_2	β_4	β_3	β_6	$\delta E_{\rm S}^{\rm n}$	$\delta E_{\rm S}^{\rm p}$	$\delta E_{\rm P}^{\rm n}$	$\delta E_{\rm P}^{\rm p}$	$\delta E_{\rm S+P}$
96	150	246	♦	0.30	0.22	0.12	0.30	−3.75	−3.73	0.54	0.93	−6.01
98	222	320	♦	0.72	−0.08	0.00	0.02	−4.65	−3.55	0.73	0.75	−6.72
102	212	314	♦	0.10	−0.38	0.00	0.26	−4.78	−3.61	0.92	0.95	−6.53
106	194	300	♦	−0.76	0.26	0.02	0.16	−1.42	−2.19	0.27	0.92	−2.42
108	162	270	♦	0.24	−0.10	0.00	−0.04	−6.45	−4.82	1.29	0.91	−9.06
122	238	360	♦	0.20	−0.16	0.00	0.08	−7.20	−0.28	1.44	0.28	−5.75
126	224	350	♦	−0.46	0.12	0.00	0.02	−3.37	−1.29	1.31	0.84	−2.51
126	238	364	♦	−0.16	0.06	0.00	0.02	−4.19	−2.19	1.30	1.03	−4.05
126	244	370	♦	− 0.20	0.10	0.00	0.00	−5.62	−1.58	1.44	0.65	−5.10
126	252	378	♦	−0.24	0.18	0.00	0.10	−3.96	−3.63	0.92	0.98	−5.69
128	310	438	♦	0.16	−0.06	0.00	−0.02	−6.65	−1.11	1.10	1.14	−5.52
130	216	346	♦	0.64	−0.30	0.00	−0.04	−4.52	−1.73	0.95	0.51	−4.79
136	244	380	♦	−0.22	0.08	0.00	0.00	−5.58	0.91	1.37	0.36	−2.94
136	282	418	♦	0.44	−0.18	0.00	0.00	−4.78	−2.23	0.95	0.94	−5.12
140	322	462	♦	0.66	−0.18	0.00	−0.06	−7.44	−1.27	1.56	0.75	−6.40
136	260	396	♦	0.36	−0.04	0.00	0.00	−3.17	−2.18	1.25	1.07	−3.03
146	260	406	♦	0.38	−0.02	0.00	−0.04	−3.17	−0.95	0.84	0.93	−2.34
146	282	428	♦	0.40	−0.16	0.00	0.00	−4.41	−1.50	0.90	0.76	−4.24
156	358	514	♦	0.34	−0.04	0.00	−0.04	−7.70	−0.85	1.46	1.25	−5.84
170	364	534	♦	−0.12	0.36	0.00	−0.02	−5.33	−2.87	0.87	0.98	−6.35
174	430	604	♦	−0.12	0.14	0.00	−0.04	−6.82	−2.04	1.47	1.08	−6.31
192	432	624	♦	−0.08	0.14	0.00	−0.04	−7.64	−1.34	1.46	1.07	−6.45
192	440	632	♦	−0.08	0.14	0.00	−0.02	−6.07	−1.57	1.52	1.04	−5.08
212	430	642	♦	−0.36	−0.02	0.00	0.04	−7.15	−0.87	1.55	1.13	−5.35
222	448	670	♦	−0.42	−0.22	0.06	−0.02	−4.86	−1.87	1.37	1.17	−4.20
222	532	754	♦	0.04	0.08	0.00	0.06	−4.10	−0.59	1.61	1.21	−1.87
230	432	662	♦	−0.12	0.14	0.00	−0.04	−6.95	−2.73	1.42	1.08	−7.17

Continued

Z	N	A	type	β_2	β_4	β_3	β_6	$\delta E_{\rm S}^{\rm n}$	$\delta E_{\rm S}^{\rm p}$	$\delta E_{\rm P}^{\rm n}$	$\delta E_{\rm P}^{\rm p}$	$\delta E_{\rm S+P}$
230	448	678	♦	0.18	0.12	0.00	0.02	−7.38	−0.18	1.46	1.09	−5.01
232	502	734	♦	0.14	−0.12	0.00	0.04	−1.82	1.91	1.35	0.76	2.21
238	448	686	♦	0.18	0.12	0.00	0.02	−7.45	−0.85	1.43	1.11	−5.76
240	452	692	♦	0.20	0.10	0.00	−0.02	−6.01	−1.05	1.46	1.19	−4.42
246	476	722	♦	0.46	−0.20	0.00	0.02	−1.46	−3.17	1.37	1.08	−2.19
88	176	264	●	−0.08	−0.04	0.00	0.00	−4.84	−1.02	0.27	0.84	−4.75
88	194	282	●	0.50	−0.12	0.00	0.02	−3.29	−1.90	0.10	0.74	−4.35
96	206	302	●	0.22	0.12	0.00	−0.02	−5.10	−2.42	1.20	0.98	−5.34
98	150	248	●	0.30	0.26	0.12	0.28	−4.75	−3.76	0.87	0.77	−6.87
106	224	330	●	0.24	−0.06	0.04	−0.08	−5.28	−3.77	0.77	0.78	−7.50
108	168	276	●	0.22	−0.12	0.00	0.02	−5.86	−3.21	1.18	0.90	−6.99
116	268	384	●	−0.24	0.40	0.00	−0.02	−0.98	−3.59	−0.65	0.97	−r4.25
126	204	330	●	0.52	−0.24	0.00	0.04	−5.97	−1.00	1.13	0.53	−5.31
126	218	344	●	0.62	−0.38	0.00	−0.06	−3.11	−1.62	1.03	0.61	−3.10
126	232	358	●	0.20	−0.10	0.00	0.02	−5.79	−0.21	1.13	1.02	−3.84
156	378	534	●	0.34	−0.12	0.00	−0.04	−8.59	−0.28	1.40	1.03	−6.44
162	300	462	●	0.06	−0.04	0.00	0.02	−3.76	−4.52	0.95	0.83	−6.51
166	314	480	●	0.04	0.08	0.00	0.04	−8.60	−4.28	1.37	0.87	−10.64
170	416	586	●	0.06	0.08	0.00	0.02	−7.41	−2.06	1.52	1.10	−6.85
196	416	612	●	0.08	0.04	0.00	−0.02	−10.45	−0.27	1.58	1.16	−7.98
212	416	628	●	0.04	0.04	0.04	0.04	−11.28	−1.70	1.48	1.04	−10.45
270	518	788	●	0.04	−0.02	0.00	0.02	−3.23	−6.05	1.19	0.82	−7.28
146	352	498	○	−0.62	0.02	0.00	0.02	−5.72	−1.92	1.12	1.01	−5.50
122	216	338	▽	0.64	−0.40	0.00	−0.04	−3.44	−2.66	1.11	0.97	−4.02
128	300	428	▽	0.64	−0.32	0.00	0.02	−5.07	−2.30	0.58	0.84	−5.95
132	294	426	▽	0.60	−0.30	0.00	0.00	−5.35	−3.30	0.91	0.97	−6.77
192	370	562	▽	−0.24	−0.18	0.00	0.00	−7.38	−1.19	1.32	0.94	−6.31
250	508	758	▽	0.10	−0.10	0.00	0.04	−3.83	1.75	1.07	1.01	0.00
80	120	200	△	−0.10	−0.08	0.00	0.00	−3.70	−5.54	−0.18	0.92	−8.50
80	162	242	△	0.26	−0.10	0.00	0.00	−5.47	0.40	1.22	0.50	−3.36
80	176	256	△	−0.10	−0.08	0.00	0.00	−5.09	−3.77	0.27	0.77	−7.82
96	222	318	△	0.70	−0.08	0.00	0.06	−5.03	−2.56	0.88	0.98	−5.73
98	206	304	△	0.22	0.12	0.00	−0.06	−4.67	−2.06	1.06	0.90	−4.76
102	162	264	△	0.24	−0.08	0.00	−0.06	−5.95	−0.89	1.33	0.01	−5.50
102	172	274	△	0.18	−0.18	0.00	0.08	−6.80	1.13	1.27	0.11	−4.30
102	192	294	△	0.58	0.34	0.00	0.02	−3.87	0.27	0.77	0.67	−2.17
108	190	298	△	−0.62	0.20	0.00	−0.06	−1.70	−2.23	0.23	0.61	−3.09
108	220	328	△	0.24	−0.08	0.02	−0.06	−4.93	−3.52	1.30	0.86	−6.28
108	240	348	△	0.18	−0.12	0.00	0.04	−7.36	−0.27	1.23	0.69	−5.70
122	206	328	△	0.48	−0.22	0.00	0.04	−6.26	−0.54	1.36	0.71	−4.74
128	268	396	△	0.38	−0.38	0.00	−0.02	−3.60	−2.93	0.88	1.02	−4.62
130	244	374	△	−0.20	0.10	0.00	0.00	−5.72	−1.25	1.41	1.04	−4.52
130	294	424	△	0.62	−0.32	0.00	0.02	−4.89	−3.39	0.77	0.94	−6.58
132	310	442	△	0.66	−0.28	0.00	0.00	−6.13	−2.53	0.85	1.02	−6.79
146	252	398	△	−0.24	0.24	0.22	−0.10	−2.59	−2.20	1.13	0.92	−2.73
146	324	470	△	0.72	−0.16	0.00	0.10	−7.72	−1.44	1.29	1.08	−6.79
162	378	540	△	0.36	−0.14	0.04	0.00	−8.37	−0.50	1.42	1.20	−6.26
178	400	578	△	0.06	−0.06	0.00	0.02	−9.13	1.20	1.63	0.56	−5.74
180	342	522	△	−0.10	0.22	0.00	0.08	−6.81	−2.98	1.42	1.05	−7.33
190	352	542	△	0.24	0.22	0.00	0.10	−5.58	−3.54	1.31	0.99	−6.83
196	392	588	△	0.08	−0.32	0.00	−0.02	−5.41	−2.06	1.25	0.91	−5.31

Continued

Z	N	A	type	β_2	β_4	β_3	β_6	$\delta E_{\rm S}^{\rm n}$	$\delta E_{\rm S}^{\rm p}$	$\delta E_{\rm P}^{\rm n}$	$\delta E_{\rm P}^{\rm p}$	$\delta E_{\rm S+P}$
198	416	614	△	0.08	0.04	0.00	−0.02	−10.47	−0.71	1.56	1.28	−8.34
208	502	710	△	0.32	−0.12	0.22	−0.02	1.55	−1.46	1.50	1.17	2.76
212	396	608	△	−0.04	−0.06	0.10	−0.04	−10.03	−2.38	1.43	1.06	−9.93
212	432	644	△	−0.34	−0.02	0.00	0.10	−7.27	−0.38	1.38	1.04	−5.23
222	502	724	△	0.12	−0.10	0.00	0.04	−0.78	−0.45	1.35	0.79	0.91
230	440	670	△	0.16	0.14	0.04	0.06	−8.51	−0.64	1.50	0.96	−6.69
230	476	706	△	−0.08	−0.40	0.00	0.00	−0.79	−1.45	1.34	1.21	0.32
238	532	770	△	0.04	0.10	0.00	0.02	−3.29	1.36	2.09	1.31	1.47
240	470	710	△	−0.28	−0.16	0.00	0.00	−2.39	−2.23	1.36	0.95	−2.31
240	518	758	△	−0.08	−0.08	0.00	0.00	−1.90	0.42	1.09	1.08	0.69

In Table 5, The predicted doubly magic nuclei located at the center of an island of stability which has quasi-magic proton and spherical neutron magic numbers are introduced. As indicated in Table 5, there are two groups of this type of doubly magic nuclei. One has quasi magicity signatured in both shell and pairing energy calculations, namely; $^{244}{\rm Cm}_{148}$, $^{366}{\rm Hs}_{258}$, $^{368}122_{246}$, $^{420}146_{274}$, $^{486}156_{330}$, $^{624}192_{432}$, $^{644}212_{432}$, $^{662}230_{432}$, $^{754}232_{522}$. The other group is composed of quasi-magic proton number that show magicity signatures in the pairing energy calculations, and it includes $^{216}{\rm Hg}_{136}$, $^{276}{\rm Cf}_{178}$, $^{280}{\rm No}_{178}$, $^{290}{\rm Sg}_{184}$, $^{292}{\rm Hs}_{184}$, $^{354}{\rm Hs}_{246}$, $^{326}116_{210}$, $^{362}116_{246}$, $^{350}122_{228}$, $^{336}126_{210}$, $^{366}130_{236}$, $^{492}174_{318}$.

Table 5. The same as Table. 4, but for the predicted doubly magic nuclei located at the center of an island of stability possessing quasi-magic proton and spherical neutron magic numbers. Detailed explanation of the different types of the doubly magic nuclei indicated below by the symbols ♦ and ○ are explained in detail in the text.

Z	N	A	type	β_2	β_4	β_3	β_6	$\delta E_{\rm S}^{\rm n}$	$\delta E_{\rm S}^{\rm p}$	$\delta E_{\rm P}^{\rm n}$	$\delta E_{\rm P}^{\rm p}$	$\delta E_{\rm S+P}$
96	148	244	♦	0.28	0.20	0.12	0.16	−3.64	−3.28	0.25	0.66	−6.01
108	258	366	♦	−0.02	0.00	0.08	0.00	−10.70	0.28	1.78	1.04	−7.60
122	246	368	♦	−0.20	0.14	0.00	0.06	−4.70	−3.91	1.18	0.80	−6.63
146	274	420	♦	0.38	−0.12	0.00	−0.04	−3.90	−1.61	1.18	0.75	−3.58
156	330	486	♦	0.06	−0.08	0.06	0.02	−5.60	−1.77	1.36	1.02	−4.99
192	432	624	♦	−0.08	0.14	0.00	−0.04	−7.64	−1.34	1.46	1.07	−6.45
212	432	644	♦	−0.34	−0.02	0.00	0.10	−7.27	−0.38	1.38	1.04	−5.23
230	432	662	♦	−0.12	0.14	0.00	−0.04	−6.95	−2.73	1.42	1.08	−7.17
232	522	754	♦	−0.04	−0.06	0.00	−0.02	−4.46	1.52	0.92	1.19	−0.84
80	136	216	○	0.62	−0.24	0.00	0.00	−3.53	−2.32	0.53	0.46	−4.86
98	178	276	○	0.06	−0.02	0.10	0.02	−4.81	0.73	0.84	0.78	−2.46
102	178	280	○	−0.12	−0.04	0.00	0.04	−6.35	1.81	1.39	0.38	−2.76
106	184	290	○	−0.60	0.20	0.00	−0.04	−3.13	−3.38	1.18	0.86	−4.47
108	184	292	○	−0.60	0.20	0.00	0.00	−2.91	−3.08	1.10	0.93	−3.96
108	246	354	○	0.10	−0.10	0.00	0.08	−8.14	0.56	1.69	0.55	−5.35
116	210	326	○	−0.10	−0.36	0.00	−0.06	−3.49	−1.34	1.05	1.04	−2.74
116	246	362	○	0.02	0.12	0.00	−0.08	−5.88	−3.42	1.05	0.80	−7.45
122	228	350	○	−0.40	0.08	0.00	−0.02	−2.37	−3.37	1.02	0.87	−3.84
130	236	366	○	0.18	−0.10	0.00	0.04	−5.83	1.11	1.24	0.59	−2.89
174	318	492	○	0.08	0.08	0.00	−0.06	−7.29	−1.68	1.36	0.91	−6.69

In Table 6, we present the predicted doubly magic nuclei located at the center of an island of stability which has spherical proton magicity and quasi-magic neutron numbers. As indicated in Table 6, there are three groups of these doubly magic nuclei, categorized according to the evidence of magicity. The first group, indicated by "♦", are doubly magic nuclei in which the quasi magicity are signatured in both shell and pairing energy calculations; this includes $^{242}{\rm U}_{150}$, $^{304}{\rm U}_{212}$, $^{320}120_{200}$, $^{326}120_{206}$, $^{530}178_{352}$, $^{542}178_{364}$, $^{528}186_{342}$, $^{708}244_{464}$, $^{752}244_{508}$. The second group is indicated by "○", and it contains doubly magic nuclei with neutron quasi magicity

are signatured only in the pairing energy calculations, namely $^{362}114_{248}$, $^{376}120_{256}$, $^{388}124_{264}$, $^{438}138_{300}$, $^{430}154_{276}$, $^{444}154_{290}$, $^{456}154_{302}$, $^{476}154_{322}$, $^{524}154_{370}$, $^{532}154_{378}$, $^{514}172_{342}$, $^{510}178_{332}$, $^{578}178_{400}$. The last group, indicated by "●", contains doubly magic nuclei with neutron quasi magicity which are signatured only in the shell energy calculations namely; $^{232}Pb_{150}$, $^{296}U_{204}$, $^{558}172_{386}$.

Table 6. The same as Table.4, but for the predicted doubly magic nuclei located at the center of an island of stability possessing spherical proton magicity and quasi-magic neutron numbers. Detailed explanation of the different types of these doubly magic nuclei indicated below by the symbols ♦, ○ and ● are explained in details in the text.

Z	N	A	type	β_2	β_4	β_3	β_6	$\delta E_{\rm S}^{\rm n}$	$\delta E_{\rm S}^{\rm p}$	$\delta E_{\rm P}^{\rm n}$	$\delta E_{\rm P}^{\rm p}$	$\delta E_{\rm S+P}$
92	150	242	♦	0.24	0.20	0.00	0.26	−3.11	−4.05	0.57	0.91	−5.69
92	212	304	♦	0.20	0.20	0.00	0.28	−4.32	−3.63	0.45	0.81	−6.69
120	200	320	♦	0.54	−0.38	0.00	−0.04	−3.10	−3.25	0.87	0.76	−4.72
120	206	326	♦	0.50	−0.24	0.00	0.06	−5.85	−0.79	1.37	0.97	−4.30
178	352	530	♦	−0.12	0.26	0.00	0.04	−5.21	−4.02	1.23	0.79	−7.22
178	364	542	♦	−0.18	0.40	0.00	−0.02	−5.12	−2.56	0.86	1.14	−5.69
186	342	528	♦	0.20	0.14	0.00	−0.04	−4.82	−2.97	1.10	1.00	−5.69
244	464	708	♦	−0.30	−0.18	0.00	0.00	−3.41	−1.73	1.50	1.04	−2.61
244	508	752	♦	0.10	−0.10	0.00	0.04	−3.55	2.37	1.09	0.98	0.89
114	248	362	○	0.12	−0.14	0.00	0.08	−6.40	−3.13	0.84	0.88	−7.82
120	256	376	○	0.00	0.00	0.04	0.00	−6.26	−1.33	0.99	1.06	−5.54
124	264	388	○	0.42	−0.40	0.00	0.02	−3.24	−3.07	0.67	0.77	−4.87
138	300	438	○	0.54	−0.22	0.00	−0.04	−4.57	−3.42	0.90	0.93	−6.16
154	276	430	○	−0.24	−0.22	0.00	−0.12	−3.19	−1.48	1.08	0.81	−2.78
154	290	444	○	0.48	0.04	0.00	0.00	−2.72	−2.70	1.17	0.92	−3.33
154	302	456	○	−0.02	−0.04	0.10	−0.02	−4.44	−3.70	1.38	0.89	−5.86
154	322	476	○	0.70	−0.14	0.00	0.04	−5.85	−3.42	0.90	0.80	−7.57
154	370	524	○	0.36	−0.10	0.00	−0.06	−9.04	0.09	1.57	0.82	−6.56
154	378	532	○	0.36	−0.14	0.00	−0.02	−8.99	0.28	1.38	0.73	−6.60
172	342	514	○	−0.06	0.22	0.00	0.02	−6.76	−2.99	1.35	0.95	−7.45
178	332	510	○	−0.14	0.18	0.00	0.04	−5.70	−3.91	1.35	0.86	−7.41
178	400	578	○	0.06	−0.06	0.00	0.02	−9.13	1.20	1.63	0.56	−5.74
82	150	232	●	0.64	−0.04	0.00	0.06	−2.80	−1.27	−0.07	0.71	−3.42
92	204	296	●	0.18	0.18	0.00	0.08	−6.25	−2.94	1.50	0.76	−6.92
172	386	558	●	0.38	−0.18	0.00	0.06	−8.13	−0.27	1.20	0.92	−6.27

To further clarify on the positions of the proposed deformed doubly magic numbers away from the stability line, their imbalance of protons and neutrons, and also the strength of their magicity signatures, in Fig. 11 we plotted the shell-plus-pairing energy of the predicted doubly magic nuclei as a function of the Neutrons From Stability (NFS) defined as:

$$\mathrm{NFS} = N - Z - 0.4A^2/(A+200) \tag{21}$$

The dashed horizontal line indicated in Fig. 11 represents the average value of the shell-plus-pairing energy of the doubly magic nuclei that reads -5.06 ± 2.37 MeV. The symbols ♦, ●, ○ △ and ▽ indicates the confirmation evidence on deformed doubly magicity; the symbols are the same as used in Table 4. The NFS has an average of 25.9, and around 76% of the predicted doubly magic nuclei have NFS below 41, which is almost midway between the maximum and minimum values of the NFS variable. The dominance and the strength of the proton magicity at $Z = 108$ (Hassium isotopes) is remarkable. The isotopes $^{270}Hs_{162}$, $^{276}Hs_{168}$, $^{292}Hs_{184}$, $^{298}Hs_{190}$, $^{328}Hs_{220}$, $^{348}Hs_{240}$, $^{354}Hs_{246}$ and $^{366}Hs_{258}$ are found to have deformed doubly magicity with NFS of −98, −92, −76, −70, −40, −20, −14 and −2 respectively. Among the predicted deformed doubly magic nuclei, $^{580}166_{314}$, and $^{628}212_{416}$ are the deepest points in the shell-plus-pairing energy space with = −10.64 MeV and −10.45 MeV, respectively. Moreover, they have small values of NFS variable that are way below the NFS average of 12.47 and 13.48, respectively.

It is important to note here that the Strutinsky method relies on the assumption that the realistic shell correction can be inferred uniquely from an independent-particle model whose single-particle levels close to the Fermi energy fit the experimental data. The Strutinsky approach converges very well when it is applied to infinite

depth potentials such as the harmonic oscillator potential or a Nilsson model potential, and one can always find an interval for both the energy smoothing parameter and the order of the curvature-correction polynomial where the shell correction practically remains the same [70, 77]. On the other hand, complications arise in calculations using finite depth potentials where the number of bound levels above the Fermi energy is not enough for the application of the energy-averaging method [6, 7, 70, 71, 75]. The effect of the particle continuum is especially important for drip line nuclei where the Fermi-level is close to zero and the nucleons can be easily excited into the continuum [73, 74, 76, 78, 79]. However, the lack of systematic studies using the continuum level density is arguably due to the fact that these calculations are quite cumbersome. In Ref. [72], Kruppa pointed out that for deformed single-particle potentials, the continuum level density has a very complicated form and one has to determine the S-matrix by solving the coupled system of differential equations for each value of single particle energy. In practice, this is quite a difficult task to perform [77].

In our results, among all the predicted doubly magicity, $^{366}\mathrm{Hs}_{258}$ is found to be the closest deformed doubly magic nucleus to the two neutron dripline with neutrons of -2 from the two neutron dripline. In fact, the magicity at Z=108 and N= 258 have been previously reported in many studies. For instance, using self-consistent calculations, D. Kolb predicted $N = 258$ to be a magic number for neutrons that is found to be fairly stable against changes in Z in the region close to the neutron dripline [69]. Also, in Ref. [31], the magicity at $N = 258$ is reported based on relativistic continuum Hartree-Bogoliubov calculations with different interactions. Furthermore, as explained earlier, Z=108 is proven to have deformed magicity in the vicinity of N = 162 [14–19]. The prediction of a deformed island of stability around $^{366}\mathrm{Hs}_{258}$ together with experimentally confirmed magicity such as $^{270}\mathrm{Hs}_{162}$ nucleus raises the confidence and confirms the reliability of the results and the adapted methodology used in this study, especially in the extrapolated regions.

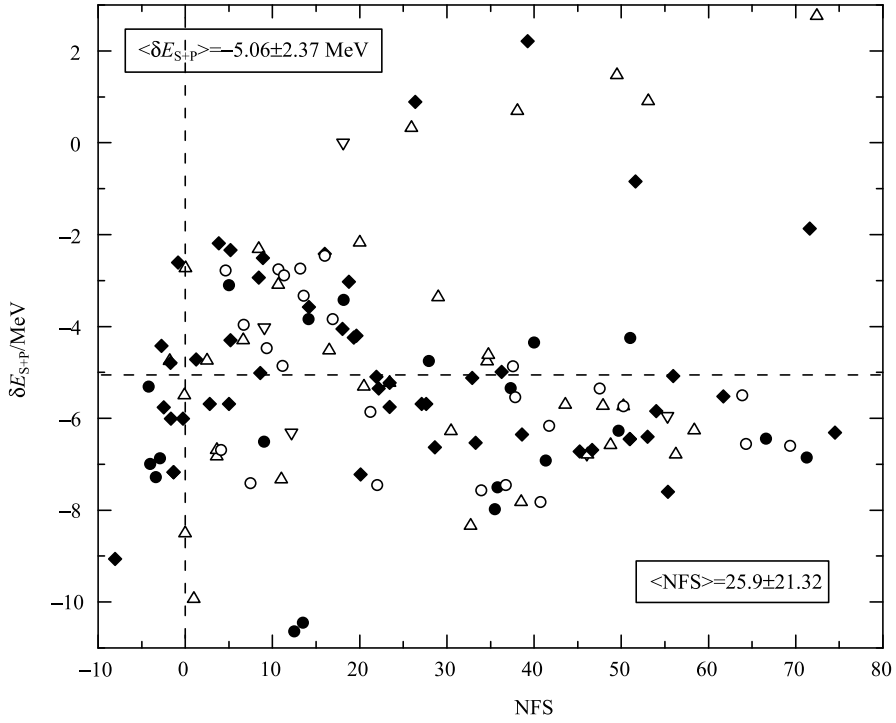

Fig. 11. The shell-plus-pairing energy $\delta E_{\mathrm{S+P}}$ plotted as a function of the variable NFS $= N - Z - 0.4A^2/(A+200)$ for the predicted deformed doubly magic nuclei in the range $72 \leqslant Z \leqslant 282$ and $96 \leqslant N \leqslant 540$. Detailed explanation of the symbols ♦, ●, ○ △ and ▽ are explained in details in the text.

Away from the stability line different decay modes prevail (α, β^+, β^-, p and n) as we reach drip lines and instabilities dominate, especially for nuclei with $Z > 130$. Nevertheless, it is believed that the shell structure of doubly magic nuclei in super- and ultra-heavy regions is the salvage for the possible existence of such systems. The formation of predicted deformed doubly magic nuclei like $^{334}\mathrm{No}_{232}$, $^{438}128_{310}$, $^{534}156_{378}$ that are located

at the centers of possible islands of stability in the instability nuclear land close to the two neutron drip line are beyond our current reach and observations. In fact, the survival of such nuclei against instabilities needs rigorous investigation. In Ref. [62], P. Roy Chowdhury et. al have estimated the half lives of about 1700 isotopes of heavy and superheavy nuclei. Among the reported half lives, in Ref. [62], are ones for nuclei that we predict to be located at the centers of valleys of deformed stability. Using the density dependent M3Y (DDM3Y) effective nucleon-nucleon interaction, the α-decay half-lives evaluated using the theoretical Q-values from Koura-Tachibana-Uno-Yamada (KUTY) mass estimates for $^{264}No_{162}$, $^{274}No_{172}$, $^{280}No_{178}$, $^{290}Sg_{184}$, $^{300}Sg_{194}$, $^{270}Hs_{162}$, $^{276}Hs_{168}$, $^{292}Hs_{184}$, $^{298}Hs_{190}$ and $^{320}120_{200}$ are $7.63E{+}09$ s, $2.21E{+}14$ s, $2.03E{+}17$ s, $3.71E{+}15$ s, $7.54E{+}24$ s, $2.75E{+}01$ s, $2.51E{+}00$ s, $3.04E{+}12$ s , $5.51E{+}13$ s and $3.51E{+}03$ s, respectively. Thus, some of the predicted doubly magic nuclei are expected to have relatively long half lives and others have very short half lives. We believe that extrapolating our knowledge to these extreme systems can play a crucial role in our understanding of nuclear systems. Furthermore, understanding the behavior of such nuclei can integrate and be of a good help in understanding the dynamical evolution of neutron stars [63].

4 Summary and conclusion

Quasi-magic proton and quasi-magic neutron numbers for even-even nuclei with $72 \leqslant Z \leqslant 282$ and $96 \leqslant N \leqslant 540$ lying between $N_{\rm G}$-10 and two neutron drip lines are explored, and their effective ranges along the nuclear landscape where their nucleon magicity is pronounced are identified. The calculations showed that $Z = 80$, 88, 96, 98, 102, 106, 108, 116, 122, 126, 128, 130, 132, 136, 140, 146, 156, 162, 166, 170, 174, 180, 190, 192, 196, 198, 208, 212, 222, 230, 232, 238, 240, 246, 250 and 270 are the quasi-magic numbers for protons, and $N = 120$, 150, 162, 168, 172, 176, 190, 192, 194, 204, 206, 212, 216, 218, 220, 222, 224, 232, 238, 240, 244, 252, 260, 268, 274, 282, 294, 300, 310, 314, 322, 324, 342, 352, 358, 364, 370, 378, 392, 396, 400, 416, 430, 432, 440, 448, 452, 470, 476, 502, 508, 518 and 532 are the quasi-magic numbers for neutrons that contribute to the formation of deformed islands of stability.

Just as in the case for spherical magic numbers, quasi-magic numbers are not static along the nuclear landscape. We investigated these shifts in light of the contributions of forming deformed islands of stability along a wide range of the nuclear landscape in heavy, super- and ultraheavy regions, and the results were found to be just in line with what was found in Ref. [9] for spherical shell stability. The shifts in the initial pattern of the islands of stability for both quasi and spherical magicity, especially in the super and ultraheavy regions, can be argued due to the presence of large single-particle level density and also the appearance of many low-j shells around Fermi level. Although quasi-magic numbers are proved to be as important as spherical ones, quasi-magic numbers show weaker evidence in the energy calculation in comparison with that of spherical magic numbers.

Furthermore, neutron magicity is more pronounced in the energy calculations in comparison with proton magicity in both the quasi and spherical magic numbers. Arguably, this can be explained in terms of single-particle spectra, because of the sensitivity of the shell corrections to the level density in the vicinity of the Fermi energy. The average density of single-particle levels around the Fermi energy increases with particle number. As a result, the spacings of single-particle levels are expected to be much smaller than those of lighter nuclei. However, the strong Coulomb field pushes the protons apart from each other as far as possible, which yields larger radii, and in turn significant changes in the proton shell structure are produced [68]. In fact, a small relative shift of one single-particle level can result in opening up or closing a gap in the spectrum.

In the proton range $72 \leqslant Z \leqslant 282$ and neutron range $96 \leqslant N \leqslant 540$, among 5568 even-even nuclei that reside in the range between $N_{\rm G}$-10 and two neutron drip line, we identified 133 deformed doubly magic nuclei located at the centers of deformed islands of stability that vary in their depth, strength of evidence and location between $N_{\rm G}$-10 and the two neutron drip line. The proposed deformed doubly magic nuclei are $^{200}Hg_{120}$, $^{216}Hg_{136}$, $^{242}Hg_{162}$, $^{256}Hg_{176}$, $^{232}Pb_{150}$, $^{264}Ra_{176}$, $^{282}Ra_{194}$, $^{242}U_{150}$, $^{296}U_{204}$, $^{304}U_{212}$, $^{244}Cm_{148}$, $^{246}Cm_{150}$, $^{302}Cm_{206}$, $^{318}Cm_{222}$, $^{248}Cf_{150}$, $^{276}Cf_{178}$, $^{304}Cf_{206}$, $^{320}Cf_{222}$, $^{264}No_{162}$, $^{274}No_{172}$, $^{280}No_{178}$, $^{294}No_{192}$, $^{314}No_{212}$, $^{322}No_{220}$, $^{334}No_{232}$, $^{290}Sg_{184}$, $^{300}Sg_{194}$, $^{330}Sg_{224}$, $^{270}Hs_{162}$, $^{276}Hs_{168}$, $^{292}Hs_{184}$, $^{298}Hs_{190}$, $^{328}Hs_{220}$, $^{348}Hs_{240}$, $^{354}Hs_{246}$, $^{366}Hs_{258}$, $^{362}114_{248}$, $^{326}116_{210}$, $^{362}116_{246}$, $^{384}116_{268}$, $^{320}120_{200}$, $^{326}120_{206}$, $^{376}120_{256}$, $^{328}122_{206}$, $^{338}122_{216}$, $^{350}122_{228}$, $^{360}122_{238}$, $^{368}122_{246}$, $^{388}124_{264}$, $^{330}126_{204}$, $^{336}126_{210}$, $^{344}126_{218}$, $^{350}126_{224}$, $^{358}126_{232}$, $^{364}126_{238}$, $^{370}126_{244}$, $^{378}126_{252}$, $^{396}128_{268}$, $^{428}128_{300}$, $^{438}128_{310}$, $^{346}130_{216}$, $^{366}130_{236}$, $^{374}130_{244}$, $^{424}130_{294}$, $^{352}132_{220}$, $^{426}132_{294}$, $^{442}132_{310}$, $^{380}136_{244}$, $^{396}136_{260}$, $^{418}136_{282}$, $^{438}138_{300}$, $^{462}140_{322}$, $^{398}146_{252}$, $^{406}146_{260}$, $^{420}146_{274}$, $^{428}146_{282}$, $^{470}146_{324}$, $^{498}146_{352}$, $^{430}154_{276}$, $^{444}154_{290}$, $^{456}154_{302}$, $^{476}154_{322}$, $^{524}154_{370}$, $^{532}154_{378}$, $^{486}156_{330}$, $^{514}156_{358}$, $^{534}156_{378}$, $^{462}162_{300}$, $^{540}162_{378}$, $^{480}166_{314}$, $^{534}170_{364}$, $^{586}170_{416}$, $^{514}172_{342}$, $^{558}172_{386}$, $^{492}174_{318}$, $^{604}174_{430}$, $^{510}178_{332}$, $^{530}178_{352}$, $^{542}178_{364}$, $^{578}178_{400}$, $^{522}180_{342}$, $^{528}186_{342}$, $^{542}190_{352}$, $^{562}192_{370}$, $^{624}192_{432}$, $^{632}192_{440}$, $^{588}196_{392}$, $^{612}196_{416}$, $^{614}198_{416}$, $^{710}208_{502}$, $^{608}212_{396}$, $^{628}212_{416}$, $^{642}212_{430}$, $^{644}212_{432}$, $^{670}222_{448}$, $^{724}222_{502}$, $^{754}222_{532}$, $^{662}230_{432}$,

$^{670}230_{440}$, $^{678}230_{448}$, $^{706}230_{476}$, $^{734}232_{502}$, $^{754}232_{522}$, $^{686}238_{448}$, $^{770}238_{532}$, $^{692}240_{452}$, $^{710}240_{470}$, $^{758}240_{518}$, $^{708}244_{464}$, $^{752}244_{508}$, $^{722}246_{476}$, $^{758}250_{508}$ and $^{788}270_{518}$.

Although some of the predicted nuclei are far from the current experimental reach, extrapolating our knowledge to these extreme systems can play a crucial role in our understanding of nuclear systems. Furthermore, understanding the behavior of such nuclei can integrate and be of a good help in understanding the dynamical evolution of neutron stars [63]. More accurate descriptions of nuclear systems can never be achieved without experimental evidence of nuclear magicity and other structural properties for the heaviest systems and this would decrease the number of models and the different parameterizations in nuclear theory, revealing more of the reality of the yet mysterious nuclear systems.

References

1 P. Doornenbal, H. Scheit, S. Takeuchi et al, Phys. Rev. Lett., **111**: 212502 (2013)
2 S. Hofmann, Rep. Prog. Phys., 61:639 (1998).
3 S. Hofmann and G. Münzenberg, Rev. Mod. Phys., **72**: 733 (2000)
4 A. Bohr and B. R, in *Mottelson. Nuclear Structure*, Vol. 2(New York, 1975)
5 I. Muntian, Z. Patyk, and A. Sobiczwski, Phys. Lett., B, **500**: 241 (2001)
6 V. M. Strutinsky, Nucl. Phys., A, **95**: 420 (1967)
7 V. M. Strutinsky, Nucl. Phys. A, **122**: 1 (1968)
8 Robert Smolańczuk, Phys. Rev. C, **56**: 812 (1997)
9 M. Bender, W. Nazarewicz, and P.-G. Reinhard, Phys. Lett. B, **515**: 42 (2001)
10 U. Mosel and W. Greiner, Z. Phys., **217**: 256 (1968)
11 S. G. Nilsson, C. F. Tsang, S. Szymański, S. Wycech, C. Gustafson, I. Lamm, P. Möller, B. Nilsson, and A. Sobiczewski, Nucl. Phys. A, **131**: 1 (1969)
12 A. V. Afanasjev and S. Frauendorf, Phys. Rev., C, **71**: 024308 (2005)
13 A. V. Afanasjev and S. Frauendorf, Phys. Scr., T **125**: 62 (2006)
14 Z. Patyk and A. Sobiczewski, Nucl. Phys. A, **533**: 132 (1991)
15 P. Möller and J.R. Nix, J. Phys. G, **20**: 1681 (1994)
16 S. Hofmann, V. Ninov, F. P. Hessberger, P. Armbruster, H. Folger, G. Münzenberg, H. J. Schött, A. G. Popeko, A. V. Yeremin, A. N. Andreyev, S. Saro, R. Janik, and M. Leino. Z, Phys. A, **350**: 281 (1995)
17 S. Hofmann, V. Ninov, F. P. Hessberger, P. Armbruster, H. Folger, G. Münzenberg, H. J. Schött, A. G. Popeko, A. V. Yeremin, S. Saro, R. Janik, and M. Leino, Z. Phys. A, **354**: 229 (1996)
18 Yu. A. Lazarev et al, Phys. Rev. C, **54**: 620 (1996)
19 Yu. Ts. Oganessian et al, Phys. Rev. C, **79**: 024608 (2009)
20 G. Lalazissis, M. Sharma, P. Ring, and Y. Gambhir, Nucl. Phys. A, **608**: 202 (1996)
21 S. Ćwiok, J. F. Dobaczewski, Magierski P. and Nazarewicz W. Heenen, P. H. Nucl. Phys. A, **611**: 211 (1996)
22 K. Rutz, M. Bender, T. Bŕvenich, T. Schilling, P.-G. Reinhard, J. A. Maruhn, W. Greiner, and J. A. Phys. Rev. C, **56**: 238 (1997)
23 J. Dudek, Z. Szymaśki, and T. Werner, Phys. Rev. C, **23**: 920 (1981)
24 Haifei Zhang, Jianmin Dong, Nana Ma, G.Royer, Junqing Li, and Hongfei Zhang, Nucl. Phys. A, **929**: 38 (2014)
25 M. Bender, K. Rutz, P.-G. Reinhard, J. A. Maruhn, and W. Greiner. Phys. Rev. C, **60**: 034304 (1999)
26 T. Bürvenich, K. Rutz, M. Bender et al, Eur. Phys. J, A **3**: 139 (1998)
27 A. T. Kruppa, M. Bender, W. Nazarewicz et al. Phys. Rev. C, **61**: 034313 (2000)
28 M. Brack and C. Pauli, Nucl. Phys. A, **207**: 401 (1973)
29 A. Bohr and B. R. Mottelson, Nuclear Structure, vol. **1** (W.A. Benjamin, New York, 1969)
30 C. K. Ross and R.K.Bhaduri, Nucl. Phys. A, **188**: 566 (1972)
31 W. Zhang, J. Meng, S. Q. Zhang, L. S. Geng, and H. Toki, Nucl. Phys. A, **753**: 106 (2005)
32 M. Ismail, A. Y. Ellithi, A. Adel, and Hisham Anwer, J.Phys. G, **43**: 015101 (2016)
33 M. Ismail, A. Y. Ellithi, A. Adel, and Hisham Anwer, Int. J. Mod. Phys. E, **25**: 1650004 (2016)
34 M. Brack, J. Damgaard, Pauli H.C, Strutinsky V. M, and Wong C. Y. Jensen, A.S, Rev. Mod. Phys., **44**: 320 (1972)
35 R. D. Woods and D. S. Saxon, Phys. Rev., **90**: 577 (1954)
36 K. T. R. Davies and J. R. Nix, Phys. Rev., C **14**, 1977 (1976)
37 S. Ćwiok, J. Dudek, J. Nazarewicz, J. Skalski, and J. Werner, Comput. Phys. Commun., **46**: 379 (1987)
38 F. Garcia, O. Rodriguez, J. Mesa, J. D. T. Arruda-Neto, V. P. Likhachev, E. Garrote, R. Capote, and F. Guzmán, Comput. Phys. Commun., **120**: 57 (1999)
39 A. Faessler, Ismail M, Ohtsuka N, and Wadia W. Rashdan, M. Z. Phys. A, **333**: 153 (1989)
40 A. Bohr, Mottelson B. R., and Pines D, Phys. Rev., **110**: 936 (1958)
41 S. Fujita and Godoy S, *Quantum Statistical Theory of Superconductivity*. Hingham, Mass., USA: (Kluwer Academic Publishers, 1996)
42 H. Nakada and K. Sugiura, Prog. Theor. Exp. Phys., **033D02**: 2 (2014)
43 V. Yu. Denisov, Phys. At. Nucl., **68**: 1133 (2005)
44 P. Möller, J. R. Nix, W.D. Myers, and W.J. Świątecki, At. Data Nucl. Data Tables, **59**: 185 (1995)
45 P. Möller, W. D. Myers, W. J. Świątecki, and J. Treiner, Atomic Data Nucl. Data Tables, **39**: 225 (1988)
46 G. Audi, A.H. Wapstra, and C. Thibault, Nucl. Phys., A, **729**: 337 (2003)
47 S. Goriely, M. Samyn, and J.M. Pearson, Phys. Rev., C **75**, 064312 (2007)
48 M. Kowal, P. Jachimowicz, and J. Skalski, submitted to Atomic Data and Nuclear Data Tables, (available from nucl-th:**1203.5013v1**), (2012)
49 O. Sorlin and M.-G. Porquet, Prog. Part. Nucl. Phys., **61**: 602 (2008)
50 D. N. Basu, Int. J. Mod. Phys., E **13**: 747 (2004)
51 M. Ismail and A. Adel, Int. J. Mod. Phys. E, **21**: 1250062 (2012)
52 C. Scheidernberger, F. Attallah , K. Beckert, F. Bosch, H. Eickhoff, M. Falch et al, in *Proceedings of the International Conference on Nuclear Physics* (Dubna, Russia, 1999)
53 Roger A. Rydin, Nuclear Science and Engineering, **179**: 352 (2015)
54 J. H. Hamilton, Hofmann S., and Oganessian Y.T, Journal of Physics: Conference Series, **580**: 012019 (2015)
55 H. F. Zhang, Y. Gao, N. Wang, J. Q. Li, E. G. Zhao, and G. Royer, Phys. Rev. C **85**: 014325 (2012)
56 Yu. Oganessian, Acta Phys. Pol. B, **43**: 167 (2012)
57 R. K. Gupta, S. Dhaulta, R. Kumar, M. Balasubramaniam, G.

Munzenberg, and W. Scheid, Phys. Rev. C, **68**: 034321 (2003)
58 S. Liran, A. Marinov, and N. Zeldes, Hyperfine Interactions, **132**: 421 (2001)
59 D. N. Poenaru and Greiner W, *Heavy Elements and Related New Phenomena*, Vol II. Singapore: (World Scientific, 1999)
60 Raj K. Gupta, *Heavy Elements and Related New Phenomena*, Vol II. Singapore: (World Scientific, 1999)
61 T. Sil, S. K. Patra, B. K. Sharma, M. Centelles, and X. Vinas, Phys. Rev. C, **69**: 044315 (2004)
62 P. Roy Chowdhury, C. Samanta, and D. N, Basu. Atomic Data Nucl. Data Tables, **94**: 781 (2008)
63 K. H. Bennemann and J. B. Ketterson, *Novel Superfluids*, Volume 2 (New York: Oxford University Press, 2014)
64 A. A. Saldanha, A. R. Farhan, and M. M. Sharma, J. Phys., G **36**: 115103 (2009)
65 A. Staszczak, A. Baran, and W. Nazarewicz, Phys. Rev. C, **87**: 024320 (2013)
66 J. Dobaczewski, A. V. Afanasjev, M. Bender, L. M. Robledo, and Yue Shi. Nucl. Phys. A, **944**: 388 (2015)
67 S. E. Agbemava, A. V. Afanasjev, T. Nakatsukasa, and P. Ring, Phys. Rev. C, **92**: 054310 (2015)
68 M. Bender and P-H. Heenen, J. Phys.: Conf. Ser., **420**: 012002 (2013)
69 D. Kolb, Z. Phys. A, **280**: 143 (1977)
70 V. M. Strutinsky, F. A. Ivanjuk, and V. V. Pashkevich, Sov. J. Nucl. Phys, **31**: 46 (1980)
71 V. M. Strutinsky, Yad. Fiz., **3**: 614 (1966)
72 A. T. Kruppa, Phys. Lett. B, **431**: 237 (1998)
73 F. A. Ivanyuk, V. M. Strutinsky, Z. Phys. A, **286**: 291 (1978)
74 F. A. Ivanyuk, V. M. Strutinsky, Z. Phys. A, **290**: 107 (1979)
75 F. A. Ivanyuk, Z. Phys. A, **316**: 233 (1984)
76 A. Bhagwat, X. Vinas, M. Centelles, P. Schuck, and R. Wyss, Phys. Rev. C, **86**: 044316 (2012)
77 T. Vertse, A. T. Kruppa, and W. Nazarewicz, Phys. Rev. C, **61**: 064317 (2000)
78 W. Nazarewicz, T. R. Werner, and J. Dobaczewski, Phys. Rev. C, **50**: 2860 (1994)
79 J. Dobaczewski, W. Nazarewicz, T. R. Werner, J. F. Berger, C. R. Chinn, and J. Decharge, Phys. Rev. C, **53**: 2809 (1996)